



Glassy Carbon Microelectrode Arrays Enable Voltage-Peak Separated Simultaneous Detection of Dopamine and Serotonin Using Fast Scan Cyclic Voltammetry

Journal:	<i>Analyst</i>
Manuscript ID	AN-ART-03-2021-000425.R2
Article Type:	Paper
Date Submitted by the Author:	11-May-2021
Complete List of Authors:	<p>Castagnola, Elisa; University of Pittsburgh, Bioengineering; San Diego State University College of Engineering</p> <p>Thongpang, Sanitta; University of Washington, Departments of Electrical & Computer Engineering, Rehabilitation Medicine, and Physiology & Biophysics</p> <p>Hirabayashi, Mieko ; San Diego State University, NanoFAB. SDSU Lab, Department of Mechanical Engineering</p> <p>Nava, Giorgio; University of California Riverside, Mechanical Engineering Department, Materials Science and Engineering Program</p> <p>Nimbalkar, Surabhi ; San Diego State University, NanoFAB. SDSU Lab, Department of Mechanical Engineering</p> <p>Nguyen, Tri ; San Diego State University, NanoFAB. SDSU Lab, Department of Mechanical Engineering</p> <p>Galindo, Sandra; San Diego State University, NanoFAB. SDSU Lab, Department of Mechanical Engineering</p> <p>Oyawale, Alexis; San Diego State University, NanoFAB. SDSU Lab, Department of Mechanical Engineering</p> <p>Bunnell, James; San Diego State University, NanoFAB. SDSU Lab, Department of Mechanical Engineering</p> <p>Moritz, Chet; University of Washington, Departments of Electrical & Computer Engineering, Rehabilitation Medicine, and Physiology & Biophysics</p> <p>Kassegne, Sam; San Diego State University, NanoFAB. SDSU Lab, Department of Mechanical Engineering</p>

1
2
3
4
5
6
7
8
9
10
11
12
13
14
15
16
17
18
19

Glassy Carbon Microelectrode Arrays Enable Voltage-Peak Separated Simultaneous Detection of Dopamine and Serotonin Using Fast Scan Cyclic Voltammetry

20 *Elisa Castagnola^{a, e†*}, Sanitta Thongpang^{b,c,e}, Mieko Hirabayashi^{a,e}, Giorgio Nava^d, Surabhi*
21 *Nimbalkar^{a,e}, Tri Nguyen^{a,e}, Sandra Lara ^{a,e}, Alexis Oyawale^{ae}, James Bunnell^{ae}, Chet Moritz^{b,e},*
22 *Sam Kassegne^{a,e*}*

26
27 ^a NanoFAB. SDSU Lab, Department of Mechanical Engineering, San Diego State University,
28
29 San Diego, CA, USA

31 ^b University of Washington, Departments of Electrical & Computer Engineering, Rehabilitation
32
33 Medicine, and Physiology & Biophysics, Seattle, WA

35
36 ^c Department of Biomedical Engineering, Faculty of Engineering, Mahidol University, Nakorn
37
38 Pathom, Thailand

40
41 ^d Department of Mechanical Engineering, University of California, Riverside, Riverside, CA,
42
43 USA,

45
46 ^e Center for Neurotechnology (CNT), Bill & Melinda Gates Center for Computer Science &
47
48 Engineering; Seattle, WA 98195, USA

49
50 * corresponding authors:

51
52
53 Elisa Castagnola, Bioengineering Department, University of Pittsburgh, 3051 Fifth Ave.
54
55
56
57
58
59
60

1
2
3 Pittsburgh, PA 15260 Email: elc118@pitt.edu Tel: 412-3780720
4
5

6 Sam Kassegne • Professor of Mechanical Engineering, NanoFAB.SDSU Lab, Department of
7 Mechanical Engineering, College of Engineering, San Diego State University, 5500 Campanile
8 Drive, CA 92182-1323. E-mail: kassegne@sdsu.edu • Tel: (760) 402-7162.
9
10
11
12

13
14 KEYWORDS Glassy Carbon, Neural Probes, Microelectrode Arrays, C-MEMS, Fast Scan
15
16 Cyclic Voltammetry, *in vivo* Neurotransmitter Detection, Dopamine, Serotonin, Simultaneous
17
18 Detection
19

20 21 **ABSTRACT**

22
23 Progress in real-time, simultaneous *in vivo* detection of multiple neurotransmitters will help
24 accelerate advances in neuroscience research. The need for development of probes capable of
25 stable electrochemical detection of rapid neurotransmitter fluctuations with high sensitivity and
26 selectivity and sub-second temporal resolution has, therefore, become compelling. Additionally, a
27 higher spatial resolution multi-channel capability is required to capture the complex
28 neurotransmission dynamics across different brain regions. These research needs have inspired the
29 introduction of glassy carbon (GC) microelectrode arrays on flexible polymer substrates through
30 carbon MEMS (C-MEMS) microfabrication process followed by a novel pattern transfer
31 technique. These implantable GC microelectrodes provide unique advantages in electrochemical
32 detection of electroactive neurotransmitters through the presence of active carboxyl, carbonyl, and
33 hydroxyl functional groups. In addition, they offer fast electron transfer kinetics, capacitive
34 electrochemical behavior, and wide electrochemical window. Here, we combine the use of these
35 GC microelectrodes with the fast scan cyclic voltammetry (FSCV) technique to optimize the co-
36 detection of dopamine (DA) and serotonin (5-HT) *in vitro* and *in vivo*. We demonstrate that using
37 optimized FSCV triangular waveform at scan rates ≤ 700 V/s and holding and switching at
38 potentials of 0.4 and 1V respectively, it is possible to discriminate voltage reduction and oxidation
39 peaks of DA and 5-HT, with 5-HT contributing distinct multiple oxidation peaks. Taken together,
40 our results present a compelling case for a carbon-based MEA platform rich with active functional
41
42
43
44
45
46
47
48
49
50
51
52
53
54
55
56
57
58
59
60

1
2
3 groups that allows for repeatable and stable detection of electroactive multiple neurotransmitters
4 at concentrations as low as 1.1 nM.
5
6

7 **1. Introduction**

8
9

10 Innovative neural probes are becoming increasingly critical for both uncovering fundamental
11 principles in neuroscience and providing therapeutic intervention in a variety of neurological
12 disorders¹⁻³. Recent progress in clinical neuromodulation and brain computer interfaces (BCIs)
13 have been enabled by substantial progress in signal recording and stimulation hardware to
14 continuously monitor the nervous system subsequently deliver appropriate stimulation for closed-
15 loop control⁴⁻⁷. Further, the development of implantable multi-modal probes capable of reading
16 and writing not only electrophysiological but also electrochemical neural signals⁸⁻¹⁰ may become
17 a key enabler of understanding brain function.
18
19
20
21
22
23
24
25
26
27
28
29

30 A variety of electrochemical techniques have been used to monitor neurotransmitter levels *in vivo*
31 ¹¹⁻¹⁵. Among these, fast scan cyclic voltammetry (FSCV) is preferred due to its sub-second scale
32 high temporal resolution (hundreds of millisecond range) that is consistent with scale of chemical
33 fluctuations at neuronal synapses¹⁶⁻²⁰. For the past 30 years, FSCV has been commonly used in
34 combination with carbon fiber electrodes (CFEs) that exhibit excellent spatial resolution with
35 minimal tissue damage and inflammatory response due to their small size (7-10 μm in diameter)
36 ²⁰⁻²². However, these CFEs often lack in selectivity and experience signal degradation over a period
37 of time due to biofouling²²⁻²⁴. They are also typically limited to a single-site recording^{19, 22, 25},
38 even though there have been several reported attempts to improve their spatial resolution by
39 fabricating CFE arrays that have shown promising electrochemical detection and physiological
40 recordings²⁶⁻²⁸. Their fabrication, however, consists of a time-consuming manual process that do
41 not allow for facile batch-fabrication high-density arrays. On the other hand, several strategies
42
43
44
45
46
47
48
49
50
51
52
53
54
55
56
57
58
59
60

1
2
3 have been adopted to both improve the selectivity of specific neurotransmitters and decrease
4 electrode biofouling. These include the functionalization of CFEs with charged polymers²⁹⁻³², size
5 exclusion membranes^{33, 34}, or even *sp*³-hybridized carbon materials^{19, 35-37}, or FSCV waveform
6 optimization^{22, 23, 38}. However, despite some promising improvements in selectivity and anti-
7 fouling properties, real-time simultaneous detection of multiple neurotransmitter concentrations *in*
8 *vivo* using FSCV remains a challenge, in particular for dopamine (DA) and serotonin (5-
9 hydroxytryptamine, 5-HT) - two of the key electrochemical analytes in the central nervous system.
10 This task is further complicated by the fact that, with fast scan rates, both DA and 5-HT have
11 similar oxidation potentials that makes distinguishing them difficult^{19, 22}.

12
13
14
15
16
17
18
19
20
21
22
23
24
25 This is unfortunate because the simultaneous detection of DA and 5-HT *in vivo* in real time and
26 the study of their interactions stands out as an area of significant research interest. However, except
27 the early works of Swamy et al. who reported simultaneous detection *in vivo* using CNT-modified
28 CFEs¹⁹ and Zhou et al.³⁹ who performed in striatal slices using bare CFEs, the literature in
29 simultaneous detection of these neurotransmitters *in vivo* is very sparse. In both cases, DA and 5-
30 HT presented an oxidation peak at the same potential, but they can be differentiated by their
31 reduction peak.

32
33
34
35
36
37
38
39
40
41
42 Therefore, to address these challenges and allow the integration of multi-site neurochemical
43 detection into multimodal closed-loop systems, progress is required in developing (a) materials
44 rich with electrochemically-active functional groups and good adsorption characteristics, (b)
45 microfabrication techniques that yield array of implantable carbon-based microelectrode arrays
46 (MEAs) for multisite measurements, and (c) electrochemical measurement protocols optimized
47 for improved sensitivity and selectivity in an environment of complex kinetics of neuronal
48 chemicals on microelectrode surfaces.

1
2
3 From the perspective of the development of materials and fabrication processes to satisfy highly
4 sensitive multi-site measurement, we recently introduced a pattern transfer technology for the
5 integration of glassy carbon (GC) microelectrodes, pre-microfabricated on silicon wafer through
6 a high-temperature carbon-MEMS process, with flexible polymer substrates^{4, 40}. An advantage of
7 this process is the potential to batch-fabricate implantable GC MEAs in a highly reproducible way,
8 opening significant opportunities for a wider use of GC microelectrodes in neural applications. GC
9 has subsequently emerged as a compelling material for microelectrodes of neural probes. Indeed,
10 our previous works have demonstrated that GC MEAs are capable of high-quality
11 electrophysiological recording and stimulation with outstanding electrochemical stability^{4, 40-43}.
12 These GC MEAs also have also show to be able to detect DA with higher sensitivity compared to
13 CFEs due to the presence of numerous edge planes rich in functional groups⁴. Thus, the GC MEAs
14 open up the possibility for integrated multimodal electrophysiological and electrochemical
15 measurement on the same arrays^{4, 40}.
16
17
18
19
20
21
22
23
24
25
26
27
28
29
30
31
32
33

34 A fundamental understanding of the mechanisms driving adsorption of electroactive species, such
35 as DA and 5-HT, on GC microelectrode surfaces will help develop optimized detection protocols.
36 Here, we investigate the electrochemical kinetics of DA and 5-HT at planar GC microelectrodes
37 using a variety of FSCV waveforms to optimize co-detection of DA and 5-HT *in vitro* and *in vivo*.
38 To enable a better understanding of adsorption/desorption kinetics of DA, 5-HT and their
39 combination, we also investigate the use of multi-waveform FSCV (*M-FSCV*), a powerful
40 technique that provides additional information on adsorption/desorption characteristics of
41 neurotransmitters⁴⁴.
42
43
44
45
46
47
48
49
50
51
52

53 **2. Materials and Methods**

54
55
56
57
58
59
60

2.1 Microfabrication

We microfabricated a 4-channel penetrating neural probes on flexible polymeric substrate with a total shank length of 7 mm (and 0.5 mm width) for targeting the rat striatum and four GC microelectrode detection sites (1500 μm^2 area), positioned in the striatum, with an inter-electrode distance of 220 μm as shown in Figure 1 a.

The core extended C-MEMS microfabrication technology used for the fabrication of the GC microelectrode arrays supported on polymeric substrates is described in detail elsewhere^{40, 42, 43}. This recently introduced technique consists of a pattern transfer method that enabled the incorporation of pre-patterned GC microelectrodes on flexible polyimide substrate, expanding the use of GC technology to implantable neural probes suited for electrophysiological and electrochemical recordings and electrical stimulation⁴. Here, we further extend the functionality of this microfabrication technology by adding a reinforcing layer to allow easy penetration of brain tissue, in order to target deep brain regions^{40, 41}.

In summary, the microfabrication process involves spin-coating SU8 negative photoresist (Microchem, MA) at 1200 rpm for 55 s and soft-baking at 65°C for 10 min and 95°C for 20 min followed by UV exposure at ~ 400 mJ/cm². The post-exposure bake consists of 65°C for 1 min and 95 °C for 5 min. This was followed by development of SU8 for 3–5 min and curing at 150°C for 30 min. Pyrolysis was done at 1000°C in an inert N₂ environment following protocols described elsewhere^{43, 45}, resulting in GC microelectrodes with high graphitic content⁴⁶. Briefly, pyrolysis is carried out in a closed quartz tube-furnace under vacuum and Nitrogen atmosphere through gradual heating to 1000 °C followed by cooling to room temperature⁴⁵. After the pyrolysis step, 6 μm layer of photo-patternable polyimide (HD 4100) (HD Microsystems, DE, USA) was spin-

1
2
3 coated on top of GC microelectrodes at 2500 rpms for 45 s, soft baked at 90°C for 3 min and at
4
5 120 °C for 3 min, then cooled down to room temperature, and patterned through UV exposure at
6
7 ~400 mJ/cm². Post-exposure bake consisted of 80°C for 1 min. Development was performed using
8
9 a spray-puddle process where QZ3501 (Fuji Film, Japan) was dispersed to form a puddle on a
10
11 stationary wafer. A rinse was applied after a set time of 15 s, followed by spin-drying of the wafer
12
13 (2000 rpm for 15 s and 500 rpm s⁻¹ ramp). The spray-puddle cycle was repeated three times and
14
15 the wafer rinsed with SU8 developer (MicroChem, USA). Subsequently, the polyimide layer was
16
17 partially cured at 300°C for 60 min under a N₂ environment.
18
19
20
21

22
23 Following, metal traces were deposited using NR91000PY negative photoresist (Futurrex Inc.,
24
25 USA) as a sacrificial layer. NR91000PY was spin-coated at 500 rpm for 45 s and ramped down
26
27 for 10 s, then prebaked for 2 min at 150 °C followed by 380 mJ/cm² UV exposure. Post exposure
28
29 bake was done at 100 °C for 2 min and the sample was developed in RD6 developer (Futurrex Inc.,
30
31 USA) for 3 s. Subsequently, 20 nm Ti adhesion layer and 200 nm Pt layer was deposited through
32
33 sputtering. After metal deposition, a lift-off process was performed, and the sacrificial layer was
34
35 removed in acetone. For electrical insulation, an additional 6 μm of polyimide HD4100 (300 rpms)
36
37 was spun, patterned (400 mJ/cm²), and cured (350°C for 90 min) under N₂ environment.
38
39 Additional 30 μm thicker layer of polyimide (Durimide 7520, Fuji Film, Japan) was spin-coated
40
41 (800 rpm, 45 s) and then patterned (400 mJ/cm²) on top of the insulation layer to reinforce the
42
43 penetrating portion of the device. Then it was developed, as previously described, and final cured
44
45 at 350 °C for 90 min. Subsequently, the device was released from the wafer through selective
46
47 etching of silicon dioxide with buffered hydrofluoric acid. The probes were then connected to a
48
49 custom-built printed circuit board (PCB) that served as the connector to the FSCV system (Figure
50
51 1 a). SEM image of the glassy carbon microelectrodes is given in Supplementary Figure 1.
52
53
54
55
56
57
58
59
60

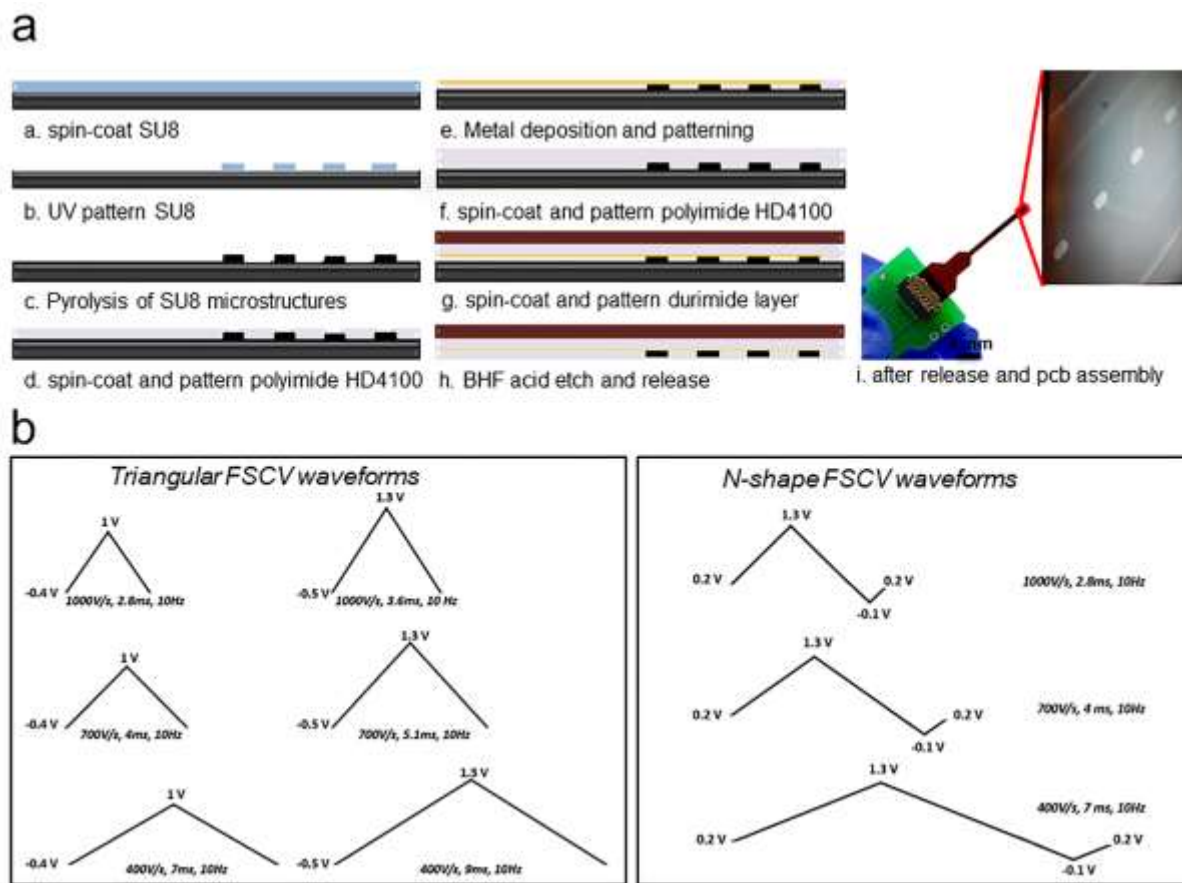


Figure 1 (a) microfabrication steps (left) and a 4-channel penetrating neural probes on polymeric substrate (right), with a total shank length of 7 mm (and 0.5 mm width) for targeting the rat striatum and four GC microelectrode detection sites ($1500 \mu\text{m}^2$ area), positioned in the striatum, with an inter-electrode distance of $220 \mu\text{m}$ (inset). The probe was connected to a custom-built printed circuit board (PCB) that served as the connector to the FSCV system. (b) FSCV electrochemical waveforms used for the DA and 5-HT detection and co-detection: triangular FSCV with EW - 0.4/1V and -0.5/1.3V at 400,700 and 1000V/s, respectively (left) and N-shaped FSCV (0.2 to 1.3 to -0.1 to 0.2 V) at 400, 400,700 and 1000V/s, respectively (right).

2.2 Simultaneous Detection and Microelectrode Kinetics Experiments

1
2
3 FSCV was performed using Wave Neuro Potentiostat System (Pine Research, NC). Data analysis
4
5 was performed using the HDCV software (UNC Chapel Hill). DA and 5-HT were identified by
6
7 inspection of the background-subtracted cyclic voltammograms (CV), performed using the HDCV
8
9 software.
10

11
12
13 As shown in Figure 1 b, we used FSCV waveforms consisting of (a) triangular FSCV waveforms
14
15 at three different scan rates (400, 700, and 1000 V/s) and two sets of holding (i.e., -0.4 and -0.5V)
16
17 and switching potentials (1 and 1.3 V). The corresponding electrochemical windows (EW) were -
18
19 0.4V/1V and -0.5V/1.3V, respectively, and (b) *N*-shaped modified FSCV waveform at 3 different
20
21 scan rate (400,700 and 1000 V/s) and holding and switching potentials of (0.2 to 1.3 and -0.1 to
22
23 0.2 V). The *N*-shaped waveform used here is a modified version of the Jackson waveform³⁸. This
24
25 waveform was designed to reduce fouling reactions of 5-HT's oxidative and reductive by-products
26
27 at CFEs, improving electrode sensitivity and stability over time^{22,38}.
28
29
30

31
32
33 Prior to the beginning of each experiment, the same voltage waveform was applied to the
34
35 microelectrodes at 60 Hz for 15-20 minutes for activating the carbon surface of the microelectrodes
36
37⁴⁷. For electrode calibration, known concentrations of DA, 5-HT, and their mixture were then
38
39 infused over 5 seconds while changes in current were recorded for 20 seconds. For the kinetics
40
41 experiments, known concentration of DA or 5-HT were injected into the PBS solution and then
42
43 changes in current were recorded for 60 seconds. For the co-detection experiments, the same
44
45 concentration of their mixture (50% DA: 50% 5-HT) was simultaneously added to the PBS
46
47 solution and then changes in current were recorded for 60 seconds.
48
49
50

51 **2.3 *In Vivo* Experiments**

52
53
54
55
56
57
58
59
60

1
2
3 **Acute FSCV Experiments in Rat Brain:** All animal experiments were performed in
4 accordance with the Association for Assessment and Accreditation of Laboratory Animal Care
5 (AAALAC) Guide for the Care and Use of Laboratory Animals (8th Edition) and approved by the
6 University of Washington Institutional Animal Care and Use Committee (IACUC) under protocol
7 number 4265-01. Adult female Long-Evans rats (250-300g) were used in this study and anesthesia
8 was induced with Urethane (1.5 g kg⁻¹, i.p., made in a 50% w/w solution in 0.9% saline). The
9 animal was placed in a stereotaxic frame and the GC probe targeting caudate-putamen (relative to
10 bregma: AP +1.2, ML +2.0, DV -4.5) and Ag/AgCl reference electrode (3.5 mm long) were placed
11 contralateral of the recording electrode (AP: -7mm, ML: -4mm) and fixed on the skull with the
12 bone cement (Polymethyl methacrylate (PMMA)). Additional hole was drilled above the
13 substantia nigra area at AP -5.6, ML +1.4, DV -8.0 for a stimulating wire electrode. The
14 dorsoventral position of the stimulating electrode was adjusted until peak and stimulated release
15 was obtained. The Ag/AgCl reference electrode was made of Ag wire (~0.5mm diameter) soaked
16 in hydrogen peroxide until a uniform AgCl layer is generated.
17
18
19
20
21
22
23
24
25
26
27
28
29
30
31
32
33
34
35

36 **Voltammetry Recording Sessions:** As described in Section 2.3, a triangle waveform was
37 applied to the GC microelectrode with ramping from - 0.4 V to 1 V and back (vs. Ag/AgCl
38 reference) at a rate of 400 V/s and frequency of 10 Hz. This waveform enabled the discrimination
39 of oxidation and reduction DA and 5-HT peaks *in vitro*. Stimulation train of 60 pulses was applied
40 at 60 Hz with 2 ms width per pulse at 250 μ A. For all studies, stimulations were performed every
41 3 minutes. After five baseline stimulations were recorded, carbidopa (25 mg kg⁻¹ in 0.9% saline,
42 i.p., Sigma Aldrich) was administered to block peripheral decarboxylases and thirty minutes later,
43 5-hydroxytryptophan (5-HTP, Sigma Aldrich) was administered (200 mg kg⁻¹ in 0.9% saline, s.c.)
44
45
46
47
48
49
50
51
52
53
54
55
56
57
58
59
60
22. was administered (200mg kg⁻¹ in 0.9% saline, s.c.)¹⁹.

2.4 Materials Characterization

TEM imaging of the synthesized GC electrodes was carried out on a Tecnai12 microscope. The carbonaceous material was removed from the substrate with a blade, dispersed into chloroform and drop-casted on a copper TEM grid (the solvent was evaporated at room temperature). The Raman Spectra of the synthesized electrode materials were recorded in the spectral range 800–3900 cm^{-1} using a micro Raman Horiba LabRam microscope (laser wavelength 532 nm, laser power 0.06 mW, 50 \times objective).

The electrochemical behavior of the microelectrodes was studied in phosphate-buffered saline solution (PBS; 0.01 M, pH 7.4; Sigma Aldrich, USA) using electrochemical impedance spectroscopy (EIS). Methods and results are reported in Supplementary section 1 and Supplementary Figure 2.

3 Results and Discussions

3.1 *In Vitro* FSCV Characterizations

In this section, we present the outcomes of the *in vitro* electrochemical sensing performance of the GC microelectrodes for the detection of DA, 5-HT and their mixture using FSCV, a background-subtracted electrochemical technique capable of measure small changes in neurotransmitter concentration.

We focus on the evaluation of the adsorption kinetics of DA and 5-HT at the GC surface as a function of scan rate, holding and switching potentials (i.e. electrochemical windows), and holding potential time, in order to obtain a better DA and 5-HT peak discrimination, following the subtraction of the capacitive background current

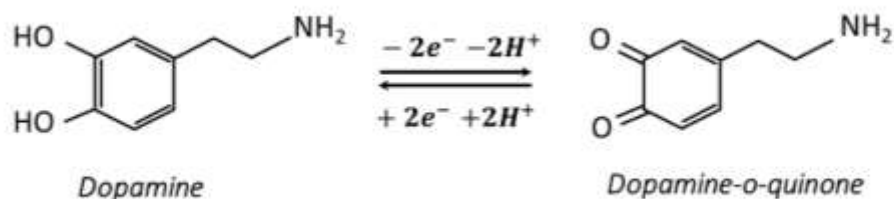
1
2
3 For *in vitro* electrochemical kinetics experiments, we used low concentrations of DA and 5-HT
4 (10 nM - 200 nM). This selection was guided by the high sensitivity of the GC microelectrodes.
5
6 Based on the linear regression slope of the maximum faradaic oxidation current versus
7
8 concentration plots, the sensitivity is determined to be (a) 164 nA/ μ M (DA) and 110 nA/ μ M (5-
9
10 HT) using EW -0.4/1 V at 400V/s and (b) 354 nA/ μ M (DA) and 170 nA/ μ M (5-HT) using EW -
11
12 0.5/1.3 V at 400V/s. In all cases, the average calibration plot (\pm SD, n = 10) follows a linear trend
13
14 in the 10 nM - 1 μ M range (see Supplementary Figure 3 a, b). The theoretical lower detection limit
15
16 (LOD), defined as 3 times the standard deviation of the noise,^{30, 48-53} was estimated to be 1.11 and
17
18 1.29 nM for DA and 5-HT respectively, when using EW -0.4/1V at 400 V/s. Similarly, LOD was
19
20 estimated to be 1.17 nM for DA and 1.73 nM for 5-HT respectively, when using EW -0.5/1.3V at
21
22 400 V/s. Based on this quantification, the GC microelectrodes are capable for the detection and
23
24 quantification of phasic DA and 5-HT levels in different brain areas^{19, 54-56}.
25
26
27
28
29
30

31 32 **3.1.1 Separate Detection of Dopamine and Serotonin**

33
34

35 First, experiments on separate detection of DA and 5-HT are presented to help understand the
36
37 adsorption kinetics of these two neurochemicals at GC microelectrodes. Particular focus is placed
38
39 on identifying their oxidation and reduction peaks using different FSCV waveforms and how these
40
41 peaks are influenced by scan rates and voltage sweep ranges, i.e. holding and switching potentials.
42
43 This will guide the adoption of the most appropriate FSCV waveform that will result in separate
44
45 and distinct peaks corresponding to DA and 5-HT.
46
47
48
49

50 DA is an electroactive neurotransmitter that electrochemically oxidizes in a two-electron
51
52 oxidation described by the equation: $DA \rightarrow DOQ + 2e^- + 2H^+$, where DOQ is the *o*-quinone form
53
54 of DA^{44, 57} (Scheme 1).
55
56
57
58
59
60



15 Scheme 1: two-electron, two-proton oxidation of dopamine.

16
17
18 DA is typically detected with FSCV through a waveform commonly called “*the dopamine*
19 *waveform*”, where a holding potential of -0.4 V is applied to the working electrode to selectively
20 preconcentrate cationic DA on the electrode surface^{35, 58, 59}. Then, a triangular waveform with a
21 scan rate of 400 V/s is applied at 10 Hz to scan the electrode to a switching potential of $+1/+1.3$ V
22 and back to -0.4 V to oxidize dopamine and reduce *dopamine-o-quinone*^{22, 35, 58}. The 10 Hz
23 frequency guarantees 100 ms temporal resolution, sufficient for capturing rapid neurotransmitter
24 release in the brain^{22, 58}. The overall current response consists of a small Faradaic current and a
25 much larger background capacitive charging current that is proportional to the scan rate. Thus,
26 FSCV requires a background subtraction method to obtain the background-subtracted CV, which
27 identify the oxidoreduction peaks of the electroactive compound^{22, 60}.
28
29
30
31
32
33
34
35
36
37
38
39
40
41

42 The GC microelectrodes generate a stable background current that enables easy identification of
43 the oxidation and reduction peaks of DA by inspection of the background-subtracted CV (Figure
44 2). The non-background-subtracted capacitive background CV plots at the different scan rates and
45 EW taken in consideration are reported in Supplementary Figure 4a.
46
47
48
49
50
51

52 As shown in Figure 2 a, FSCV using triangular waveforms (10 Hz) for DA, the separation between
53 reduction and oxidation peaks (ΔE) was observed to increase with higher scan rates, shifting the
54
55
56
57
58
59
60

1
2
3 oxidation peaks to the right and the reduction peaks to the left, respectively (Figure 2 a,
4 Supplementary Figure 5 a). The DA oxidation and reduction peak potentials at the different scan
5 rates and the corresponding ΔE are reported in Table 1, for the EW of -0.4/1 V. Using a scan rate
6 of 1000V/s in the same EW, it is not possible to obtain a proper discrimination of the oxidation
7 and reduction peaks (Figure 2 a). Further, these ΔE increase at 1000 V/s is observed for all DA
8 concentrations, EW, and FSCV waveforms used (Supplementary Figure 4 a-c, Supplementary
9 Figure 6 d-f). This is due to the insufficient time available for completion of DA oxidation under
10 fast scan rates in the range of thousands of V/s^{60,61}, likely because of the sluggish electron transfer
11 kinetics for dopamine at carbon electrodes⁶². For higher scan rates in the thousands of V/s range,
12 other possible factors include uncompensated ohmic drop and the higher current density, that
13 distort the shape of the voltammogram and cause a higher overpotential.^{62,63}
14
15
16
17
18
19
20
21
22
23
24
25
26
27
28

29 Furthermore, with scan rate of 400 V/s, a distinct shift in both oxidation and reduction peaks
30 was observed between FSCV at -0.4V/1V (0.65±0.05V, -0.22±0.03V, $\Delta E = 0.87\pm 0.05$) and the
31 wider EW of -0.5V/1.3V (0.79±0.01V, -0.35±0.01V, $\Delta E = 1.14\pm 0.06$ V), informing that peaks are
32 also functions of the EW (Supplementary Figure 5, Supplementary Figure 6). Fouling test in the
33 presence of DA was performed using the triangular waveform at scan rate of 400V/s. The current
34 peak amplitudes in response to 50 nM of DA presented small oscillation (ca. 20%) over the entire
35 recording sessions, both for reduction and oxidation peaks. Additionally, no significant drifting
36 was observed in the FSCV capacitive charging background during FSCV recording over a period
37 of 25 minutes, demonstrating the electrochemical stability of the GC surfaces (Supplementary
38 Figure 7).
39
40
41
42
43
44
45
46
47
48
49
50
51
52
53
54
55
56
57
58
59
60

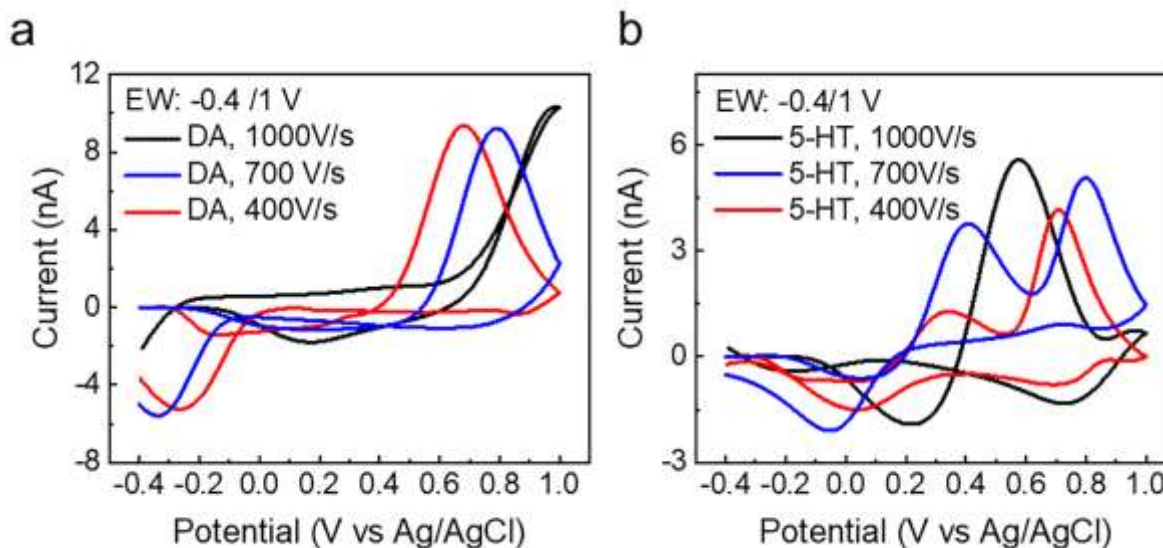


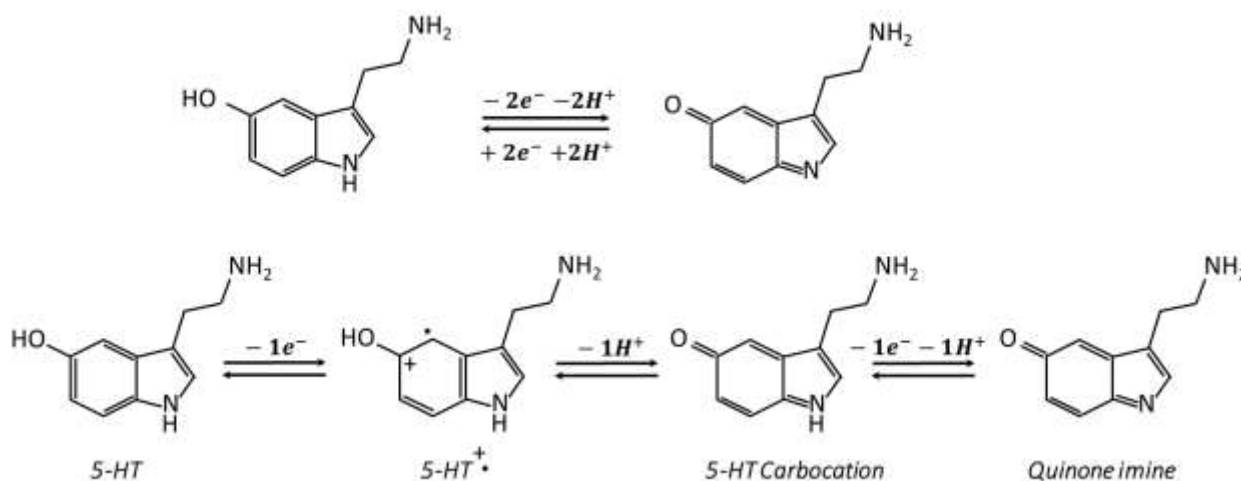
Figure 2. Effect of scan rate on DA and 5-HT kinetics using -1/0.4 V EW. (a) Effect of scan rate. DA concentration at 10 nM, 1000V/s, oxidation peak (Ox) > 1V, reduction peak (Redx) < -0.4V (black line); 700 V/s, Ox = 0.78 ± 0.03 V, Redx = -0.30 ± 0.05 V (blue line); 400 V/s, Ox = 0.65 ± 0.05 V, Redx = -0.22 ± 0.03 V, (red line), (b) Effect of scan rate on 5-HT (10 nM) oxidation peaks. While two separate oxidation peaks are observed at lower scan rates (≤ 700 V/s), these peaks merge for scan rate of 1000 V/s. The CV plots correspond to the average of 5 repetitions on 3 different electrodes (see Table 1 and Table 2).

DA	Oxidation Peak (nA)	Redox Peak (nA)	ΔE (V)
700V/s small EW	8.86 ± 0.74 --	-5.47 ± 0.45	1.04 ± 0.05
400V/s small EW	8.28 ± 1.46	-4.87 ± 0.84	0.87 ± 0.05
1000V/s small EW	--	--	--

Table 1: Mean and Standard Deviation (N=3, 5 repetitions each) of the amplitudes of 10 nM dopamine oxidation and reduction peaks and the corresponding peak separation (corresponding to Figure 2 a)

5-HT, just like DA, is an electroactive neurotransmitter that can be electrochemically oxidized within the physiological pH solvent window (Scheme 2)⁶⁴. Its oxidation reaction mechanism

involves a multi-step two-electron, two-proton transfer process^{38, 65, 66}, during which by-products such as reactive carbocation intermediate and dimers are formed (Scheme 2)^{38, 64, 65}. The Electro-oxidation mechanism of 5-HT has been extensively studied by Wrona *et. al* under acidic^{64, 67} and physiological conditions⁶⁴. They proposed that oxidation happens in a series of steps where 5-HT is oxidized first to its carbocation, followed by a further oxidation to *quinone imine* as shown in Scheme 2^{64, 67}.



Scheme 2. Mechanism of serotonin oxidation on carbon electrode surfaces adapted from⁶⁸ (top); and two step oxidations proposed and experimentally validated by Wrona *et al.*^{64, 67} (bottom).

Since this reaction dominates at fast scan rates⁶⁴, more recent literature have shown that this is the primary reaction that occurs at scan rates of 300 - 1000V/s^{65, 69, 70}. However, subsequent reactions of the carbocation with 5-HT produce dimers (5,5'-Dihydroxy-4,4'-bitryptamine, 3-(2-Aminoethyl)-3-[3'-(2-aminoethyl)-indol-5-one-4'-yl]-5-hydroxyindolenine, and 5-[[3-(2-Aminoethyl)-1H-indol-4-yl]oxy]-3-(2-aminoethyl)-H-indole)⁶⁴. The by-products have been

shown to be very reactive and adsorb irreversibly on the electrode surface resulting in fouling³⁸,⁶⁵. To overcome this difficulty, the *in vitro* and *in vivo* detections of 5-HT at CFEs are usually performed using N-shaped FSCV waveform^{38, 71}, also known as Jackson waveform³⁸, that has been optimized to accelerate electrode response times and reduce the formation of strongly adsorptive by-products. Specifically, this waveform holds the potential at +0.2 V to limit 5-HT by-product adsorption, scan quickly at 1000 V/s to 1.0 V to limit fouling, and switch down to -0.1 V to allow the detection of the reduction peak³⁸. However, this N-shaped FSCV waveform cannot be efficiently used to detect DA which needs a more negative holding potential to facilitate the cationic adsorption on the electrode surface (Supplementary Figure 6 a).

5-HT	Peak-I (nA)	Peak-II (nA)	Redox Peak (nA)	ΔE (Peak-I) (V)	ΔE (Peak-II) (V)
700V/s small EW	3.38±1.91	5.82±2.02	-2.18±0.74	0.42±0.02	0.82±0.01
400V/s small EW	2.90±1.38	5.46±1.34	-1.93±0.33	0.17±0.01	0.59±0.01
1000V/s small EW	--	5.86±0.91	-1.00±0.19	--	0.51 ±0.02

Table 2: Mean and Standard Deviation (N=3, 5 repetitions each) of the amplitudes of 10 nM serotonin oxidations (Peak I and II) and reduction peaks and the peak separations (corresponding to Figure 2 b).

As the response of 5-HT is complex and involves multi-reaction steps, the background subtracted FSCV in these experiments exhibited unique double oxidation peaks at scan rates ≤ 700 V/s. For example, as shown in Figure 2 b, for FSCV of 5-HT with EW of -0.4V/1V and 10 nM concentration, two separate oxidation peaks were observed, i.e., 0.27±0.04 (Peak-I) and 0.68±0.03V (Peak-II) for 400 V/s and 0.41±0.01V (Peak-I) and 0.79±0.02V (Peak-II) for 700 V/s scan rates. Using -0.4/1V EW at higher scan rate (1000 V/s), the two oxidation peaks seem to converge to a single peak at 0.53±0.05V (Figure 2 b). The amplitudes of 10 nM serotonin

1
2
3 oxidations (Peak I and II) and reduction peaks and the peak separations (ΔE) are reported in Table
4
5 2.

6
7
8 Using a similar waveform, the same peak at ca. 0.3–0.4 V for 5-HT has been observed at PEI/CNT
9
10 fibers⁷² and has attributed to the secondary reaction of the multi-step 5-HT oxidation described in
11
12 scheme 2⁷². This is potentially problematic since the reactive oxidation products (i.e. reactive
13
14 carbocation intermediate and dimers) of this secondary reaction of 5-HT^{38, 64, 65} have been
15
16 demonstrated to form an insulating layer on the surface of the CFEs and decrease sensitivity over
17
18 time^{38, 65}. To address the concern, we investigated the stability of 5-HT electrochemical detection
19
20 at GC microelectrode surface, where GC microelectrodes were continuously scanned in presence
21
22 of 50 nM of 5-HT and the 5-HT detection was monitored for 8 h using the triangular FSCV at 400
23
24 V/s. Every 20-40 minutes, the PBS solution containing 5-HT was changed followed by the
25
26 collection of a new background measurement and a new injection of the same 5-HT concentration.
27
28 The current peak amplitudes in response to 50 nM of 5-HT showed small oscillations over the
29
30 entire recording session, with no significant drop in detection sensitivity (one-way Anova, $p > 0.05$)
31
32 (Supplementary Figure 7). During a continuous FSCV collection, we did not observe significant
33
34 drift of the capacitive background charging current over long recording sessions (25 minutes), that
35
36 is commonly the limiting factor for long FSCV acquisitions^{16, 73, 74} (Supplementary Figure 5). This
37
38 indicates that the GC surface is stable under FSCV cycling *in vitro*, enabling the continuous
39
40 detection for the entire recording session.
41
42
43
44
45
46
47

48 For -0.5/1.3V EW, Peak-I is less defined (Supplementary Figure 5 d-e, Supplementary Figure 6 b,
49
50 c), occurring at 0.42 ± 0.05 V, 0.50 ± 0.03 V, and 0.69 ± 0.02 V for 400, 700 and 1000 V/s scan rates,
51
52 respectively. With increasing scan rate, the oxidation Peak-II shifted to the right (from 0.68 ± 0.03 V
53
54 at 400V/s to 0.78 ± 0.02 V at 700 v/s and 1.01 ± 0.01 V for 1000 V/s), while the reduction peaks
55
56
57
58
59
60

1
2
3 shifted left-wards ($0.08\pm 0.04\text{V}$, $-0.04\pm 0.01\text{V}$ and $-0.17\pm 0.01\text{V}$ for 400, 700 and 1000 V/s,
4
5 respectively) (Supplementary Figure 5 d, e). This is similar to what was observed for DA, with a
6
7 ΔE of $0.61\pm 0.03\text{V}$, $0.82\pm 0.03\text{V}$ and $1.18\pm 0.01\text{V}$ for 400, 700 and 1000 V/s, respectively
8
9 (Supplementary Figures 5 and 6). It seems, therefore, that despite the higher scan rate, the larger
10
11 EW still allows GC microelectrodes to detect the secondary oxidation peak, confirming the
12
13 influence of the EW (i.e. scan duration) and scan rate on 5-HT kinetics.
14
15

16
17
18 Using the modified *N*-shaped waveforms, only one oxidation peak was observed for all the scan
19
20 rates (Supplementary Figure 5 f). These peaks shifted towards the right with increased scan rates
21
22 (i.e., ca. 0.74, 0.90 and 1.08 V for 400, 700 and 1000V/s, Supplementary Figure 5 f). Also, the
23
24 reduction peaks seem to shift towards the right, occurring at 0.17V for 1000V/s scan rate, with ΔE
25
26 = 0.9V, suggesting a faster kinetics compared to the one using triangular waveform with 1000V/s
27
28 scan rate and same EW. However, for slower scan rates, the reduction peaks were not discriminated
29
30 using this EW because they probably appear at potentials <0.2 V. It is important to note that in
31
32 order to detect the positive oxidation peak (at 1.08V), we had to modify the traditional *N*-shaped
33
34 waveform used for 5-HT detection at CFEs by extending the switching potential to 1.2V.
35
36 (Supplementary Figure 3 f and Figure 6 a).
37
38
39
40

41
42 Further, to verify that the redox reactions of DA and 5-HT at the surface of the GC
43
44 microelectrodes are adsorption-controlled, we have plotted the oxidation peak currents versus the
45
46 scan rate for both DA and 5-HT. We observed that the current increases linearly as a function of
47
48 the scan rate, a function of the scan rate, denoting adsorption control (Supplementary Figure 9)
49
50

51 52 **3.1.2 Simultaneous Co-Detection of Dopamine and Serotonin** 53 54 55 56 57 58 59 60

Once the kinetics of DA and 5-HT was investigated separately, the simultaneous co-detection of these neurochemicals was then pursued. In this case, we ruled out the use of *N*-shaped waveform and the higher scan rate of 1000 V/s that do not allow DA detection. Instead, we focused on the triangular waveform, by varying the parameters that can influence the FSCV responses, i.e. EW, holding potential, switching potential, and scan rate^{22, 35}, to obtain the best DA and 5-HT peak discrimination, considering the electrochemical kinetics at the GC microelectrodes.

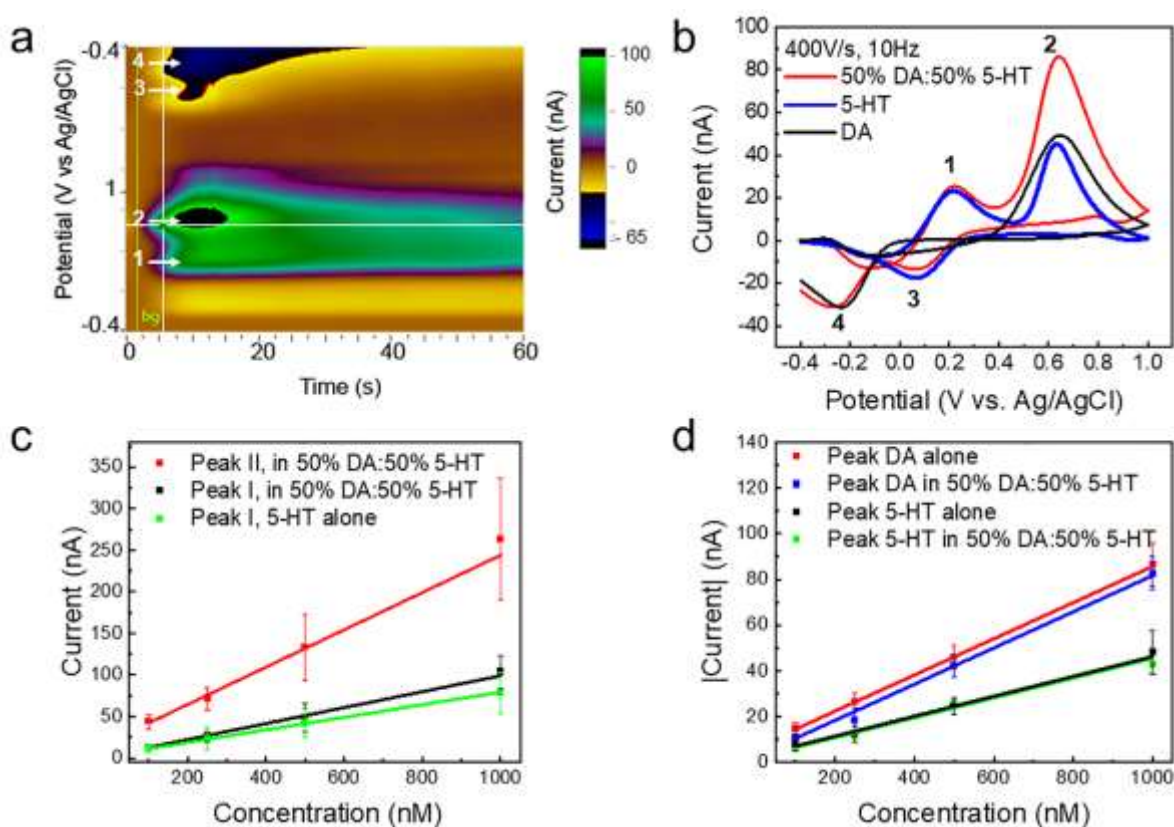


Figure 3 Simultaneous detection of DA and 5-HT using -0.4/1 V EW at 400 V/s: (a) representative color plot and **(b)** background subtracted CV for 200 nM 50 %DA: 50%5-HT mixture (red) versus DA (black), 5-HT (blue), respectively. **(c, d)** *in vitro* FSCV calibration curves of the oxidation and reduction peaks of DA and 5-HT alone and in their 50 %DA: 50%5-HT mixture. **(c)** background subtracted oxidation current of Peak I (black) and II (red) in 50 %DA:

1
2
3 50%5-HT mixture versus concentration. For comparison: background subtracted oxidation current
4 of Peak I (5-HT) alone (green). The average (n=8) sensitivity is linearly correlated. **(d)** background
5 subtracted reduction current of 5-HT Peak (green) and DA Peak (blue) in their 50 %DA: 50%5-
6 HT mixture. For comparison: background subtracted reduction current of 5- HT (black) and DA
7 Peak (red) alone. The average (n=8) sensitivity is linearly correlated.
8
9
10
11
12
13
14

15 Under 400 V/s scan rate, -0.4/1V EW, 10Hz, during DA and 5-HT mixture detection, two
16 oxidation peaks were observed (Table 3). The first oxidation was observed at $0.31\pm 0.13V$,
17 corresponding to the 5-HT oxidation Peak-I while the second one was observed at $0.67\pm 0.02V$, in
18 correspondence to 5-HT Peak-II and the DA peak (Figure 3 b). In the representative examples
19 reported in Figure 3 b, this peak represents 90 nA amplitude, that is the combination of the
20 contribution from both DA and 5-HT. Additionally, two reduction peaks were clearly observed,
21 the first at $0.09\pm 0.02 V$, corresponding to the reduction peak of 5-HT, and the second at -
22 $0.19\pm 0.02V$, corresponding to the DA reduction peaks. For comparison, see the separate DA
23 (black) and 5-HT (blue) detection plots (Figure 3 b). This marks a clear separation of the DA and
24 5-HT reduction peaks of around 300 mV. Thus, by having separate calibration for DA and 5-HT,
25 it is possible to first estimate the 5-HT concentration from the 5-HT oxidation Peak-I and reduction
26 peak, and, subsequently that of DA. The calibration curves of the oxidation and reduction peaks
27 for DA and 5-HT alone and in their 50 %DA: 50%5-HT mixture are reported in Figure 3 c, d. For
28 comparison, the background subtracted oxidation current of Peak I (5-HT) alone (green, Figure 3
29 c), 5- HT alone (black, Figure 3 d) and DA alone (red, Figure 3 d) are also presented. In all the
30 cases, the average (n=8) sensitivity is linearly correlated. Further, we do not observe a significant
31 difference between the sensitivity of 5-HT (oxidation Peak I: $80 \text{ nA}/\mu\text{M}$; reduction: $43 \text{ nA}/\mu\text{M}$)
32
33
34
35
36
37
38
39
40
41
42
43
44
45
46
47
48
49
50
51
52
53
54
55
56
57
58
59
60

and DA (reduction: 79 nA/ μ M) alone or in their mixture (oxidation Peak I: 95 nA/ μ M; reduction DA: 79 nA/ μ M; reduction 5-HT: 43 nA/ μ M).

Similar observations are made for 700 V/s scan rate and -0.4/1V EW at 10Hz (Supplementary Figure 10). Two oxidation and two reduction peaks were observed in response to the injection of 100 nM concentration of DA and 5-HT mixture. However, while the DA and 5-HT reduction peaks were well discriminated (Table 3), the 5-HT Peak-I, at 0.50 ± 0.04 , was less defined than the one for slower scan rate (Table 3).

5-HT:DA	Peak-I 5-HT (V vs Ag/AgCl)	Peak-II (DA+5- HT) (V vs Ag/AgCl)	Redox Peak 5- HT (V vs Ag/AgCl)	Redox Peak DA (V vs Ag/AgCl)
700V/s -0.4/1V EW	0.50 ± 0.04	0.84 ± 0.01	-0.09 ± 0.01	-0.34 ± 0.01
400V/s, -0.4/1 V EW	0.31 ± 0.13	0.67 ± 0.02	0.09 ± 0.02	-0.19 ± 0.01

Table 3: Mean and Standard Deviation (N=3, 5 repetitions each) of the peak position of DA and 5-HT during their simultaneous detection.

Using large EW (-0.5/1.3 V), for scan rates of 400 and 700 V/s at 10Hz, it was still possible to discriminate between the reduction peaks with a separation of ~ 300 mV. However, it was not possible to discriminate between the oxidation peaks (Supplementary Figure 11). In this case, 5-HT showed a single oxidation peak at ca. 0.66V (400V/s) and ca. 0.87 (700 V/s), where the contribution of DA and 5-HT resulted in 60 nA amplitude. This corresponds to the summation of DA and 5-HT peak amplitudes and is in agreement with a previous study which demonstrated that extended waveform reduced the chemical selectivity of DA⁷⁵.

However, equal (50:50%) concentration of DA and 5-HT are not physiological. 5-HT concentrations of electrically stimulated 5-HT are usually lower⁷⁶. For example, they are reported to be 30-100 nM in the CA2 region of the hippocampus and in the substantia nigra pars reticulata

1
2
3 of mouse brain^{54, 76}, and 130 nM in the rat striatum³⁶ after pharmacological manipulation. Instead
4
5 DA can be detected in higher concentration 250 nM³⁶ up to 1 μ M^{55, 56}, also without
6
7 pharmacological manipulation, in the striatum of rat brain. Thus, we tested DA and 5-HT mixture
8
9 at two different ratios, i.e., (60% DA and 40% 5-HT) and (75% DA and 25% 5-HT) and we
10
11 provided the evidence of this capability of GC microelectrodes in distinguishing 5-HT peaks also
12
13 when 5-HT is present is smaller concentration in the mixture (Supplementary Figure 12).
14
15
16
17

18 In summary, therefore, for -0.4/1V EW at 400 and 700 V/s scan rates, the simultaneous real-
19
20 time in vitro detection of DA and 5-HT in a 50:50 mixture solution of DA and 5-HT exhibited
21
22 double oxidation peaks, i.e. the characteristic Peak-I of 5-HT and a second peak, that is the
23
24 summation of the DA and 5-HT (Peak-II) oxidation peaks. Further, two distinct reduction peaks
25
26 were observed, each corresponding to the effects of DA and 5-HT. For larger -0.5/1.3V EW at 400
27
28 and 700 V/s scan rates it was still possible to discriminate the reduction peaks of DA and 5-HT,
29
30 but not the oxidation peaks which converged to a single one. Additionally, GC microelectrode can
31
32 distinguish 5-HT also in 75% DA and 25% 5-HT mixture.
33
34
35
36

37 **3.1.3 Effect of Multiple FSCV**

38
39
40 To further explore the reaction kinetics and adsorption/desorption characteristics of DA and 5-
41
42 HT at the surface of GC microelectrodes, we carried out multiple FSCV (*M*-FSCV) runs⁴⁴. The
43
44 adsorption of neurotransmitters from the solution on the carbon surface is well known to influence
45
46 the voltammetric responses^{44, 57, 75, 77}. For example, for DA detection using FSCV, holding a
47
48 negative potential between voltammetric sweeps has shown to improve DA adsorption on the CFE
49
50 surface, increasing the sensitivity^{44, 57, 75, 77}. Furthermore, the time at which the negative constant
51
52 potential is held in between scan repetitions, i.e. repetition time, influences the adsorption of the
53
54
55
56
57
58
59
60

1
2
3 neurotransmitter on the carbon surface^{44, 77}. Thus, considering that the adsorption behavior is
4 specific to each analyte, depending by their intrinsic properties, the study of the adsorption
5 characteristics of different neurotransmitters could help in (i) optimizing waveforms capable of
6 discrimination of various analytes and (ii) mitigating fouling. Here, we used repetition time and
7 the scan rate as parameters to study the adsorption behavior of DA and 5-HT and their differences.
8
9
10
11
12
13
14

15 First, we used a single set of *M*-FSCV scan that consisted of five consecutive triangular
16 waveforms (cycles) with a 1 ms gap between each waveform, both for DA, 5-HT, and their
17 mixtures. In this case, the duration of a singular waveform is 7 ms (EW: -0.4/1V at 400V/s), thus
18 the total scan duration, considering 1ms intervals is 39 ms and the frequency is maintained to 10
19 Hz (61 ms at the holding potential). The five consecutive FSCV waveforms were acquired by a
20 single *M*-FSCV scan, as shown in the color plots and corresponding background subtracted FSCV
21 in Figure 4 a, c, 5 a, c and 6 a, c. (Other examples are reported in Supplementary Figures 13). The
22 redox peak amplitudes of the five subsequent FSCV showed a rapidly decreasing trend, due to the
23 change in duration of the adsorption time (holding time in between cycles), from 61 ms to 1 ms.
24
25 The adsorption properties and the kinetics of DA and 5-HT at GC microelectrodes could be
26 determined from the rate of this decay. An example of color plot and background subtracted FSCV
27 of a *M*-FSCV scan in response to 20 nM DA are shown in Figure 4 a, b, c. Fast decrease in peak
28 amplitudes of the five consecutive waveforms can be observed, with a large drop of 22% noted in
29 the oxidation peak between the first and second waveform (Figure 4 d and Table 1) and an
30 exponential decay $k = 1.37$, obtained by the fitting the five consecutive DA oxidation peaks using
31 the exponential decay function $p = Ae^{-kt} + p_0$, where p is the peak amplitude at each consecutive
32 cycle, A is the initial amplitude of the exponential decay, t is the cycle number, k is a positive
33
34
35
36
37
38
39
40
41
42
43
44
45
46
47
48
49
50
51
52
53
54
55
56
57
58
59
60

constant term that describes the DA adsorption kinetics decrease with increasing scan number (Figure 4 d).

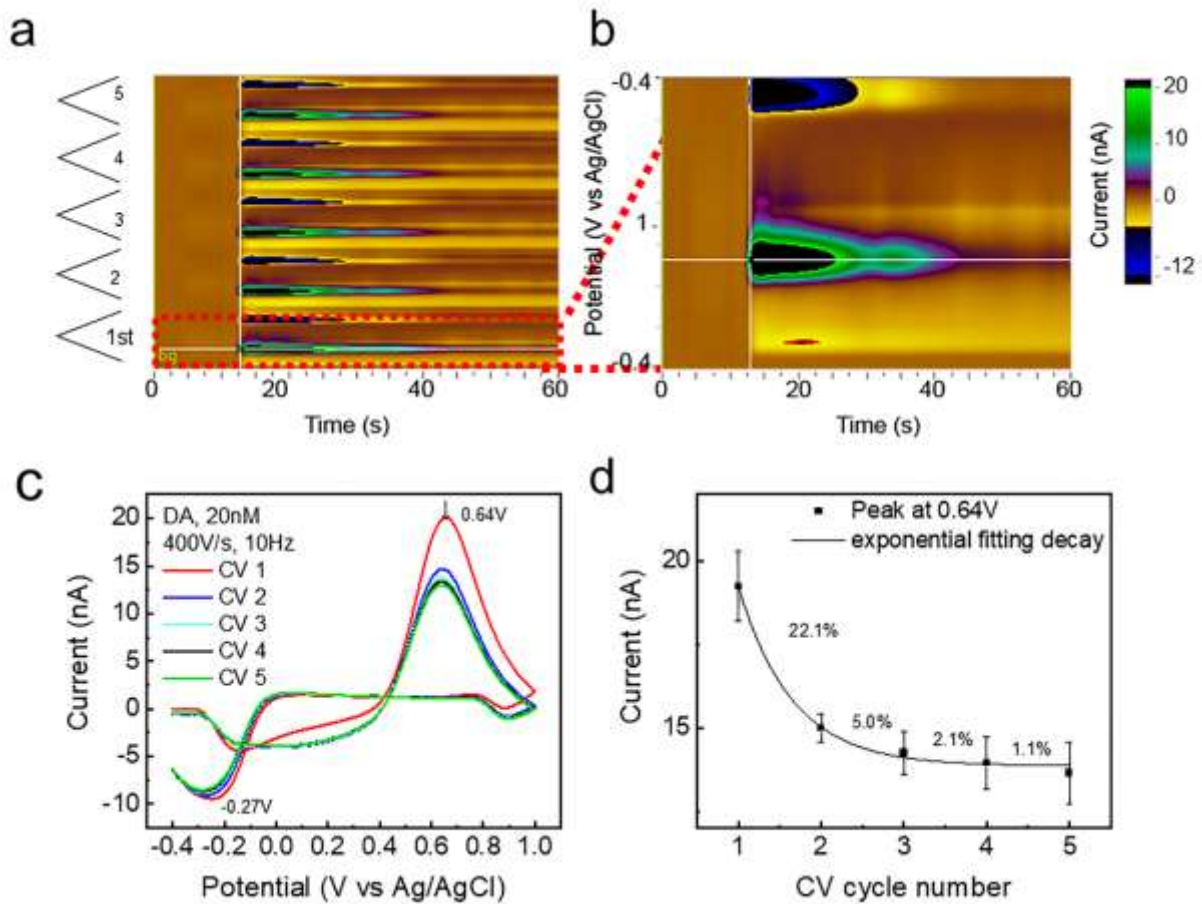


Figure 4. *M*-FSCV detection of DA at 400 V/s. A single scan in *M*-FSCV consists of five consecutive triangular waveforms with a 1 ms gap between each waveform. The duration of a singular waveform is 7 ms (EW: -0.4/1V at 400V/s), thus the total scan duration, considering the 1ms intervals, is 39 ms and the frequency is maintained to 10 Hz (61 ms at the holding potential). (a-d) 20 nM DA detection: (a) representative color plot corresponding to five consecutive FSCV waveforms acquired by a single *M*-FSCV scan with (b) magnification on the first FSCV, and (c) corresponding background subtracted CV for the five different cycle of one *M*-FSCV run. (d) percentage of the oxidation peak amplitude decay in between consecutive cycles (average and standard deviation, n=4).

The reduction peak variation is smaller, 3.8% between the first and second FSCV cycle. It is possible that the reduction current is less influenced by the holding time (also at the first scan) since the source of oxidation current is the DA adsorbed at the carbon surface during the holding time, while the source of reduction current is *DA-o-quinone* formed at the carbon surface only after the DA oxidation during the anodic sweep⁷⁷. Furthermore, it has been shown that DA adsorbs to carbon surface almost ten-fold stronger than *DA-o-quinone*⁵⁷.

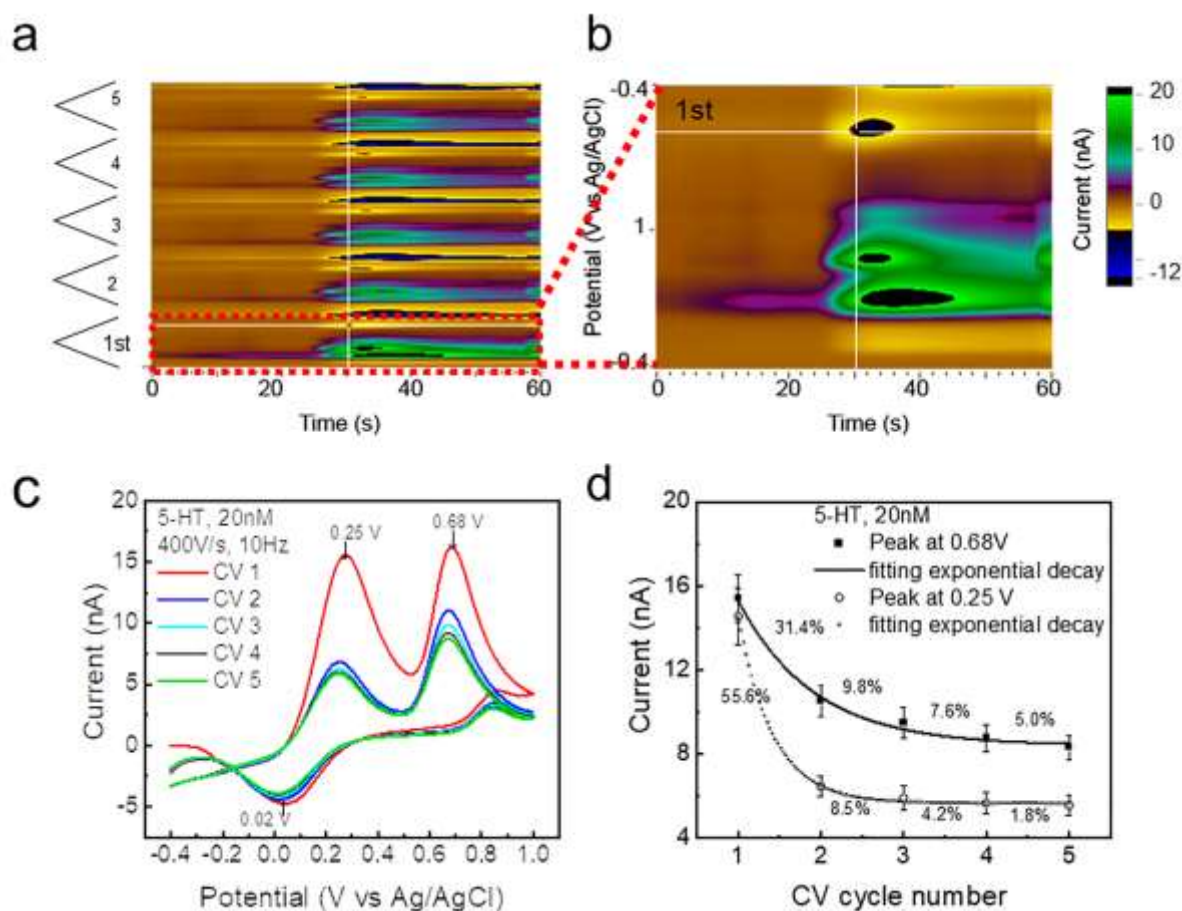


Figure 5. *M*-FSCV detection of 5-HT at 400 V/s. Single set of scans in *M*-FSCV consist of five consecutive triangular waveforms with a 1ms gap between each waveform. The duration of a singular waveform is 7 ms (EW: -0.4/1V at 400V/s). Total scan duration, considering 1 ms intervals, is 39 ms and the frequency is maintained to 10 Hz (61 ms at the holding potential). (a-d)

1
2
3 *M*-FSCV detection of 20nM 5-HT: (a) color plot corresponding to five consecutive FSCV
4 waveforms acquired by a single *M*-FSCV scan with (b) magnification on the first FSCV, and (c)
5 corresponding background subtracted CV for the five different cycle of one *M*-FSCV run. (d) The
6 percentage of the oxidation peak-I and peak-II amplitudes decay in between consecutive cycles
7 (average and standard deviation, n=4).
8
9
10
11
12
13
14

15
16 In the case of 5-HT (under the same conditions), a similar decreasing trend in peak amplitudes
17 of the five consecutive waveforms were observed. However, the decrease in oxidation and
18 reduction peak amplitudes between the first and second cycles was higher, corresponding to
19 31.4%, 55.6%, and 9.6% for the oxidation peaks at $0.68\pm 0.03\text{V}$ (Peak-II) and 0.27 ± 0.04 (Peak-I)
20 and for the reduction peak, respectively (Figure 5 d and Table 4). This rapid decay in the difference
21 of amplitude current peak with the consecutive scans ($k = 1.93$ for Peak-I and $k = 1.01$ for Peak-
22 II) suggest that 5-HT has a stronger adsorption properties compared to DA at GC microelectrodes,
23 similarly to what was reported for CFEs⁴⁴. Examples of color plots and background subtracted
24 FSCVs of a *M*-FSCV scan in response to 20 nM 5-HT are reported in Figure 5 a, b, c. Other
25 examples are reported in Supplementary Figure 13.
26
27
28
29
30
31
32
33
34
35
36
37
38
39

40 In the case of DA and 5-HT co-detection (under the same conditions), the decay of the oxidation
41 Peak-I ($0.31\pm 0.13\text{V}$) follows the 5-HT trend, with a reduction of while the oxidation Peak-II
42 ($0.65\pm 0.05\text{V}$) seems to be influenced more by the DA behavior ($k = 1.60$ for Peak-I and $k = 1.01$
43 for Peak-II). The redox peaks, at $-0.20\pm 0.05\text{V}$ and $0.09\pm 0.04\text{V}$ for DA and 5-HT respectively, are
44 well separated and do not present high degree of decay in between consecutive cycles (Table 4).
45 Examples of color plots and background subtracted FSCVs of a *M*-FSCV scan in response to 20
46 nM 5-HT are reported in Figure 5 a-c. Other examples are reported in Supplementary Figure 14.
47
48
49
50
51
52
53
54
55
56
57
58
59
60

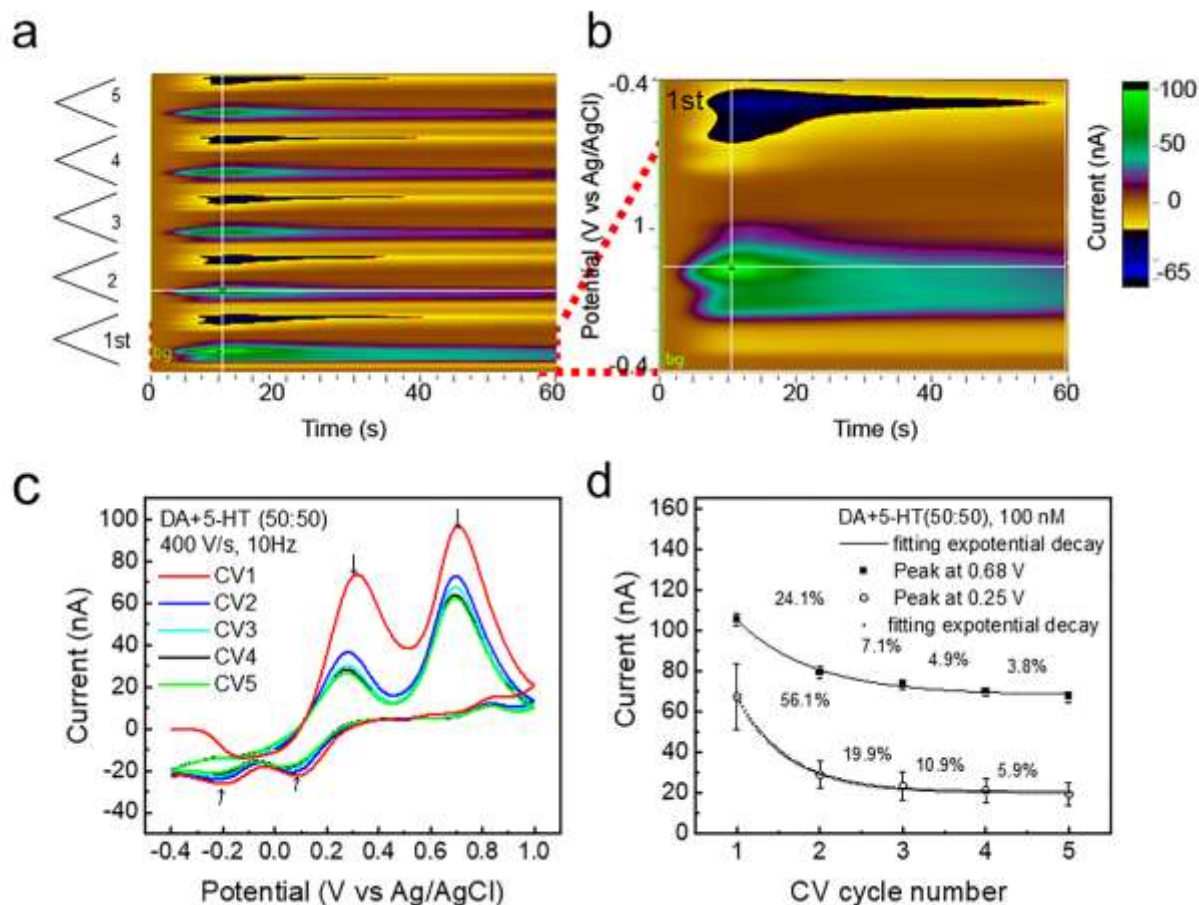


Figure 6. *M*-FSCV co-detection of DA and 5HT at 400 V/s. Single scan in *M*-FSCV consists of five consecutive triangular waveforms with a 1ms gap between each waveform. The duration of a singular waveform is 7ms (EW: -0.4/1V at 400V/s). Total scan duration, considering 1ms intervals, is 39 ms and the frequency is maintained to 10 Hz (61 ms at the holding potential). (a-d) 100nM DA+5-HT (50:50) detection: (a) color plot corresponding to five consecutive FSCV waveforms acquired by a single *M*-FSCV scan with (b) magnification on the first FSCV, and (c) corresponding background subtracted CV for the five different cycle of one *M*-FSCV run. (d) percentage of the oxidation peak amplitude decay in between consecutive cycles (average and standard deviation, n=4).

Table 4. Summary of effect of *M*-FSCV on oxidation and reduction peaks of subsequent scans.

% indicates the values after cycles in terms of the original peaks

Waveform	Scan Rate	Peak	Cycles 1-2	Cycles 2-3	Cycles 3-4	Cycles 4-5
Dopamine						
Triangular	400 V/s	Oxidation Peak 0.64 V	22.1%	5.0%	2.1%	1.1%
		Reduction Peak -0.22V	3.8%	1.9%	1.5%	0.9%
Serotonin						
Triangular	400 V/s	Oxidation Peak-II	31.4%	9.8%	7.6%	5%
		Oxidation Peak-I	55.6%	8.5%	4.2%	1.8%
		Reduction Peak	9.6%	5.3%	4.5%	1.1%
	1000V/s	Oxidation Peak	70.4%	18.8%	5.3%	4.4%
		Reduction Peak	31.2%	12.5%	8.8%	0.9%
N-Shaped	1000 V/s	Oxidation Peak	18.7%	5.1%	~ 0	~ 0
		Reduction Peak	~ 0*	~ 0	~ 0	~ 0
Dopamine + Serotonin (50:50)						
Triangular	400V/s	Oxidation Peak-II 0.65V	22.7%	6.9%	4.4%	3.5%
		Oxidation Peak-I 0.3V	55.2%	20.1%	11.2%	6.2%
		Reduction Peak (5-HT)	8.4%	4.8%	5.5%	1.3%
		Reduction Peak (DA)	11.9%	3.1%	3.2%	1.1%

For 5-HT, we also used a single set of *M*-FSCV scan that consisted of ten consecutive triangular waveforms (cycles) with a 1 ms gap between each waveform. In this case, the duration of a singular waveform is 2.8 ms (EW: -0.4/1V at 1000V/s). The total scan duration, considering the 1 ms intervals, was 37 ms and the frequency was maintained to 10 Hz (63 ms at the holding potential) (Supplementary Figure 15a and b). The ten consecutive FSCV waveforms were acquired by a single *M*-FSCV scan, as shown in the color plots and corresponding background subtracted FSCV

1
2
3 in Supplementary Figure 2a and b. The redox peak amplitudes of the ten consecutive FSCV present
4 a more drastic decrease trend, than at lower scan rate, with a ~70% reduction of the peak amplitude
5 between the first and the second cycle (see Supplementary Figure 15 a and 15 b and Table 4).
6
7 Thus, this experiment confirmed that the use of -0.4/1V triangular waveform and higher scan rate
8 increases the adsorption kinetic of 5-HT at the GC microelectrodes surface, and consequently, the
9 peak amplitude decay between consecutive FSCV scan ($k=1.95$).
10
11

12
13
14
15
16
17
18 Finally, we tested the 5-HT adsorption using a single set of *M*-FSCV scan that consisted of ten
19 consecutive N-shaped modified waveforms with a 1 ms gap between each waveform. The duration
20 of a singular waveform is also the same here with 2.8 ms (+0.2V to -1.3V to -1V at 1000V/s). The
21 total scan duration, considering the 1ms intervals, was 37 ms and the frequency was maintained to
22 10 Hz (63 ms at the holding potential). Because of the positive holding potential, the adsorption
23 was drastically reduced (Figure Supplementary Figure 16, Table 4), with a ~18% reduction of the
24 oxidation peak amplitude between the first and the second cycle and a very smooth decay.
25
26 However, as discussed earlier, this waveform cannot be used to detect DA, and hence cannot be
27 considered for simultaneous detection.
28
29
30
31
32
33
34
35
36
37
38

39 40 **3.2 *In vivo* Co-detection of Dopamine and Serotonin**

41
42
43 The proof-of-principle of *in vivo* electrochemical sensing performance of the GC
44 microelectrodes for simultaneous FSCV detection of DA and 5-HT in the rat striatum is presented
45 in Supplementary Section 2 and Supplementary Figure 17. The procedure for recording DA and
46 5-HT simultaneously was adopted from the experiments by Swamy and Venton¹⁹ and require
47 pharmacologically manipulation of the 5-HT level. Indeed, *in vivo* evoked 5-HT concentrations
48 are expected to be drastically lower than DA concentrations in the striatum^{19, 78}.
49
50
51
52
53
54
55
56
57
58
59
60

1
2
3 In summary, the preliminary results obtained validate the proof-of-concept that 5-HT and DA can
4 be simultaneously discriminated at GC microelectrodes using FSCV. This preliminary result will
5
6 serve as steppingstone for further extensive *in vivo* evaluation.
7
8
9

10 **3.3 What Drives Better Sensitivity of Glassy Carbon in Voltammetry?**

11
12 We had recently demonstrated that the lithography and the pyrolysis process of negative tone
13 epoxies such as SU-8 described here produces several discontinuous basal planes and dangling
14 carbon bonds that are rich in functional groups such as carboxyl, carbonyl, and hydroxy groups
15 that are distributed along reactive edges and defects (Figure 7 a) ^{46, 79}. These active groups,
16 particularly hydroxyl, carbonyl, and carboxy groups, are favorable for adsorption of cationic
17 species such as dopamine and serotonin whose amine side chain get protonated at physiological
18 pH.
19
20
21
22
23
24
25
26
27
28
29
30

31 Additionally, it was shown recently that the GC structure and atomic arrangement within the
32 resulting graphene edges constantly evolve at different stages of the pyrolysis process, reaching
33 maximum values for carbon pyrolyzed at around 1000 °C ^{80, 81}. At this temperature, the formation
34 of large amount of non-planar sp^2 -hybridized carbon atoms result in the evolution of stacks of
35 interconnected graphene fragments and curved graphene structures with well-defined protruding
36 facets and edge planes^{80, 81}. These stacks of graphene layers have reactive edges consisting of
37 abundant dangling bonds, non-6 membered rings, and intermediate structures in addition to defects
38 where functional groups such as carbonyl, carboxy, and hydroxyl groups attach to ^{80, 81}. On the
39 other hand, in carbon fibers that consist a stacked layer of parallel graphene sheets, the only active
40 regions come from only defect regions⁸².
41
42
43
44
45
46
47
48
49
50
51
52
53
54
55
56
57
58
59
60

1
2
3 TEM image of our electrodes is shown in Figure 7 b. In the micrograph, we can observe the
4 presence of visible curved graphene-like layers produced by the pyrolysis of SU-8 at 1000 °C⁸³.
5
6
7
8⁸⁴. The Raman spectra of the synthesized GC electrodes (see Figure 7 c) show sharp G and D
9 modes and broad but visible second order features (D', D'' and 2D' peaks), indicating a certain
10 degree of graphitization in the synthesized material (see Figure 7 c)⁸⁵. To gain better insight into
11 the material structural properties, we performed a deconvolution of the Raman spectrum using a
12 well-established fitting routine (see Figure 7 d; range 1100-1800 cm⁻¹)^{86, 87}. From the
13 deconvolution, we derived the values of the G peak position, the intensity ratio between the D and
14 G modes (I_D/I_G), and the ratio between the slope of the linear photoluminescence background
15 superimposed on the Raman spectrum and I_G . The position of the G peak (around 1605 cm⁻¹),
16 higher with respect to the values typical for amorphous carbon (e.g. 1510 cm⁻¹), and the I_D/I_G ratio,
17 which is higher than 1, point to the presence of a substantial graphitization degree and a high sp²
18 content in the GC material¹⁰². On the other hand, the low value of m/I_G (close to 0 μm) indicates
19 a low hydrogen content⁸⁷.
20
21
22
23
24
25
26
27
28
29
30
31
32
33
34
35

36 Both DA and 5-HT contain amine side chain, that are usually protonated at physiological pH
37 due to their high pKa values and have net positive charge⁸⁸⁻⁹¹. On the other hand, GC consists of
38 n-ring aromatic system. Because this ring system allows for hybridization of electron orbitals,
39 negative charges are concentrated above and below the atoms in the center of the ring which gives
40 majority of the surface of GC a slight net negative charge⁹². Further, the presence of functional
41 groups on the outer carbon rings of GC increases its overall dipole moment. Therefore, its net
42 negative charges coupled with large dipole moments increase the interaction of GC surfaces with
43 dopamine or serotonin and hence GC's capability in detecting these neurochemicals even at low
44 concentrations in the nanomolar range as shown in here and elsewhere^{4, 40}.
45
46
47
48
49
50
51
52
53
54
55
56
57
58
59
60

Therefore, with its dense edge planes that are rich with functional groups, GC is favorable for adsorption of cationic species and has demonstrated improved sensitivity for DA detection compared to CFEs^{22, 37}. Notably, defect-rich oxygen-containing carbon material surfaces have also shown an increased hydrophilicity, that help to reduce the fouling²².

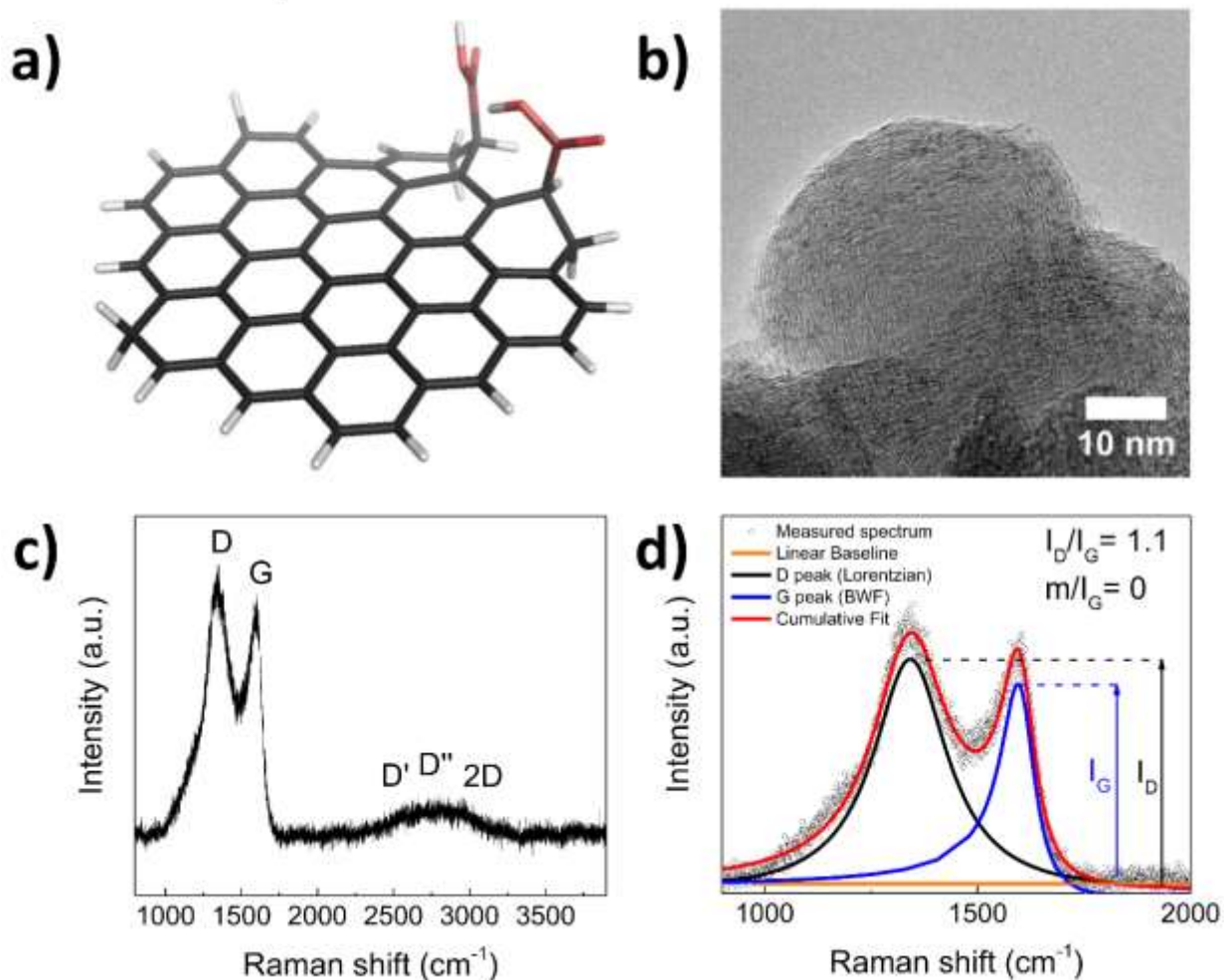


Figure 7 (a) GC structure shown with carboxylic acid functional group⁴⁶, (b) TEM of GC showing multiple basal planes that typically end with dangling carbon bonds and functional groups. (c) Raman spectrum of a GC electrode and (d) corresponding fitting scheme (one Lorentzian peak for

1
2
3 the D mode, one BWF peak for the G mode and a linear baseline). I_D and I_G are the intensities of
4
5 the D and G modes respectively.
6
7

8 9 **4. Conclusions**

10
11
12 We present an implantable GC microelectrode array supported on polymeric substrate with four
13
14 channels for *in vitro* and *in vivo* simultaneous electrochemical detection of multiple
15
16 neurotransmitters, namely, dopamine and serotonin. The probe was microfabricated through the
17
18 C-MEMS based pattern transfer technology recently developed by our group. These GC
19
20 microelectrodes have already demonstrated higher sensitivity to dopamine and serotonin due to
21
22 the numerous functional groups available on their edge planes, particularly carboxyl, carbonyl,
23
24 and hydroxyl groups that are favorable for adsorption of cationic species such as dopamine whose
25
26 amine side chain gets protonated at physiological pH. In this study, we focused on the
27
28 characterization of the electrochemical kinetics of DA and 5-HT at GC microelectrode surfaces
29
30 and gaining further insight on the adsorption/desorption mechanism of DA, 5-HT, and their
31
32 combination, using multi-waveform FSCV (*M-FSCV*).
33
34
35
36
37

38 Key findings reported in this work are:
39
40

41
42 1. We demonstrate a microfabrication and validation of a glassy carbon microelectrode array
43
44 that is rich with electrochemically active functional groups, good adsorption characteristics and
45
46 antifouling properties.
47
48

49
50 2. We demonstrate that using optimized FSCV triangular waveform at scan rates ≤ 700 V/s
51
52 and holding and switching potentials of 0.4 and 1V respectively, GC microelectrodes can
53
54
55
56
57
58
59
60

1
2
3 simultaneously discriminate *in vitro* the reduction and oxidation peaks of DA and 5-HT at low
4 concentrations (10-200nM), with serotonin contributing distinct multiple oxidation peaks.
5
6

7
8
9 3. 5-HT oxidation involves multi-reaction steps and the background subtracted FSCV of 5-
10 HT exhibits unique double oxidation peaks at scan rates ≤ 700 V/s and EW of -0.4/1V. At the same
11 EW and 1000 V/s, the two oxidation peaks seem to converge to a single peak. Using 0.5/1.3V EW,
12 the first oxidation peak is observed to be less defined with the 5-HT electrochemical kinetics at
13 GC electrodes slowing down with an increase in scan rates, similarly to what was observed for
14 DA. This confirms the influence of the EW on 5-HT kinetics.
15
16
17
18
19
20
21
22

23 4. There was no fouling detected on GC microelectrodes due to 5-HT after a long exposure
24 extending over a period of 8 h.
25
26
27
28

29 5. *M*-FSCV results demonstrate that 5-HT, compared to DA, has a stronger adsorption
30 property at GC microelectrodes, particularly at higher scan rates. Using -0.4/1V EW with scan rate
31 of 400V/s, optimal for DA and 5-HT co-detection, the decay of Oxidation-Peak-I (+0.25 V) is
32 more influence by the 5-HT trend, while Oxidation-Peak-II (+0.68V) seems influenced more by
33 the DA behavior.
34
35
36
37
38
39
40

41 6. As a proof of principle, the GC multi-array probe was implanted in the caudate putamen of
42 a rat brain in an acute experiment. The GC microelectrodes were able to discriminate DA and 5-
43 HT *in vivo*.
44
45
46
47
48

49 Taken together, the results of this study demonstrate that GC multi-array microelectrodes have a
50 compelling advantage for not only electrophysiological recording and stimulation, but also for
51 multi-site simultaneous detection of DA and 5-HT in a stable and repeatable manner. Further, the
52
53
54
55
56
57
58
59
60

1
2
3 results also demonstrate the potential of GC probes to elucidate the relationship between electrical
4 and electrochemical signaling at synapses as part of a closed neurochemical feedback loop in the
5 development of smart adaptive deep brain stimulation (DBS) systems.
6
7
8
9

10 **Supporting Information.**

11
12
13
14 Supplementary information accompanies this paper at (link)
15
16

17 **Competing Financial Interests:**

18
19
20
21 The authors declare no competing financial interests.
22
23

24 **AUTHOR INFORMATION**

25
26 Corresponding Author * Sam Kassegne • Professor of Mechanical Engineering, NanoFAB.SDSU
27 Lab, Department of Mechanical Engineering, College of Engineering, San Diego State University,
28 5500 Campanile Drive, CA 92182-1323. E-mail: kassegne@sdsu.edu • Tel: (760) 402-7162.
29
30
31
32

33 **Present Addresses**

34
35
36
37 †Elisa Castagnola Present Addresses: Department of Bioengineering, University of Pittsburgh,
38 Pittsburgh, Pennsylvania 15261, USA.
39
40
41

42 **Author Contributions**

43
44
45 **E.C.** designed and fabricated the MEA devices, performed the electrochemical detection
46 experiments, data analysis and interpretation, and wrote major part of the manuscript. **S.T.**
47 performed the in vivo validation and data analysis, **M.H.** helped with the data interpretation,
48 especially with 5-HT, **G.N.** carried out TEM measurement and wrote discussion on TEM and
49 Raman Spectroscopy. **S.N.** and **T.N.** helped in optimization and microfabrication of the MEA
50
51
52
53
54
55
56
57
58
59
60

1
2
3 devices. **S.L.** and **A.O.** performed electrochemical characterization of the devices; **J.B.** wrote
4
5 Matlab script for analyzing data. **C.M.** designed and supervised in vivo tests and revised the paper.
6
7
8 **S.K.** supervised the project, structured the outline of the paper, and wrote discussion section of the
9
10 paper.

11 12 13 **Funding Sources**

14
15
16 This work was supported by the National Science Foundation, the Center for Neurotechnology
17
18 (CNT), a National Science Foundation Engineering Research Center [Award No. EEC-
19
20 1028725].
21
22

23 24 **ACKNOWLEDGMENT**

25
26 The Authors acknowledge the support from the Center for Electron Microscopy and Microanalysis
27
28 (CFAMM) at UC Riverside for TEM measurements.
29
30

31 32 **ABBREVIATIONS**

33
34 GC, glassy carbon; MEA, microelectrode array; FSCV, fast scan cyclic voltammetry; multi-
35
36 waveform FSCV (*M-FSCV*); DA, dopamine; 5-HT, serotonin, EW, electrochemical window.
37
38

39 40 **References**

- 41 1. T. N. Lerner, L. Ye and K. Deisseroth, *Cell*, 2016, **164**, 1136-1150
42 <https://doi.org/1110.1016/j.cell.2016.1102.1027>.
- 43 2. L. A. Jorgenson, W. T. Newsome, D. J. Anderson, C. I. Bargmann, E. N. Brown, K.
44 Deisseroth, J. P. Donoghue, K. L. Hudson, G. S. Ling and P. R. MacLeish, *Philosophical*
45 *Transactions of the Royal Society B: Biological Sciences*, 2015, **370**, 20140164
46 <https://doi.org/20140110.20141098/rstb.20142014.20140164>.
- 47 3. C. T. Moritz, *Neurotherapeutics*, 2018, **15**, 628-634 [https://doi.org/610.1007/s13311-](https://doi.org/610.1007/s13311-13018-10637-13310)
48 [13018-10637-13310](https://doi.org/610.1007/s13311-13018-10637-13310).
- 49 4. S. Nimbalkar, E. Castagnola, A. Balasubramani, A. Scarpellini, S. Samejima, A.
50 Khorasani, A. Boissenin, S. Thongpang, C. Moritz and S. Kassegne, *Scientific reports*,
51 2018, **8**, 1-14 <https://doi.org/10.1038/s41598-41018-25198-x>.
- 52 5. C. A. Chapman, N. Goshi and E. Seker, *Advanced Functional Materials*, 2018, **28**,
53 1703523 <https://doi.org/1703510.1701002/adfm.201703523>.
- 54
55
56
57
58
59
60

6. K. H. Lee, J. L. Lujan, J. K. Trevathan, E. K. Ross, J. J. Bartoletta, H. O. Park, S. B. Paek, E. N. Nicolai, J. H. Lee and H.-K. Min, *Scientific reports*, 2017, **7**, 46675 <https://doi.org/46610.41038/srep46675>.
7. M. Parastarfeizabadi and A. Z. Kouzani, *Journal of neuroengineering and rehabilitation*, 2017, **14**, 79 <https://doi.org/10.1186/s12984-12017-10295-12981>.
8. A. E. Pereda, *Nature Reviews Neuroscience*, 2014, **15**, 250-263 <https://doi.org/210.1038/nrn3708>.
9. P. Alcami and A. E. Pereda, *Nature Reviews Neuroscience*, 2019, **20**, 253-271 <https://doi.org/210.1038/s41583-41019-40133-41585>.
10. A. C. Miller, L. H. Voelker, A. N. Shah and C. B. Moens, *Current Biology*, 2015, **25**, 16-28 <https://doi.org/10.1016/j.cub.2014.1010.1071>.
11. E. E. Ferapontova, *Electrochimica Acta*, 2017, **245**, 664-671 <https://doi.org/610.1016/j.electacta.2017.1005.1183>.
12. J. Njagi, M. M. Chernov, J. Leiter and S. Andreescu, *Analytical chemistry*, 2010, **82**, 989-996 <https://doi.org/910.1021/ac9022605>.
13. A. Gratton, B. J. Hoffer and G. A. Gerhardt, *Brain research bulletin*, 1988, **21**, 319-324.
14. F. Crespi, K. Martin and C. Marsden, *Neuroscience*, 1988, **27**, 885-896 [https://doi.org/810.1016/0306-4522\(1088\)90191-90191](https://doi.org/810.1016/0306-4522(1088)90191-90191).
15. S. Sharma, N. Singh, V. Tomar and R. Chandra, *Biosensors and Bioelectronics*, 2018, **107**, 76-93.
16. Y. Oh, C. Park, D. H. Kim, H. Shin, Y. M. Kang, M. DeWaele, J. Lee, H.-K. Min, C. D. Blaha and K. E. Bennet, *Analytical chemistry*, 2016, **88**, 10962-10970 <https://doi.org/10910.11021/acs.analchem.10966b02605>.
17. D. L. Robinson, B. J. Venton, M. L. Heien and R. M. Wightman, *Clinical chemistry*, 2003, **49**, 1763-1773 <https://doi.org/1710.1373/1749.1710.1763>.
18. K. M. W. a. P. Hashemi, *ACS Chem Neurosci.*, 2013, **4**, 715-720 <https://doi.org/710.1021/cn4000378>.
19. B. K. Swamy and B. J. Venton, *Analyst*, 2007, **132**, 876-884 <https://doi.org/810.1039/B705552H>.
20. Y. Ou, A. M. Buchanan, C. E. Witt and P. Hashemi, *Analytical Methods*, 2019, **11**, 2738-2755 DOI: 2710.1039/C2739AY00055K.
21. E. Castagnola, K. Woepfel, A. Golabchi, M. McGuier, N. Chodapaneedi, J. Metro, I. M. Taylor and X. T. Cui, *Analyst*, 2020, **145**, 2612-2620 <https://doi.org/2610.1039/D2610AN00051E>.
22. P. Puthongkham and B. J. Venton, *Analyst*, 2020, **145**, 1087-1102 DOI: 1010.1039/C1089AN01925A.
23. A. L. Hensley, A. R. Colley and A. E. Ross, *Analytical chemistry*, 2018, **90**, 8642-8650 DOI: 8610.1021/acs.analchem.8648b01976.
24. W. Harreither, R. Trouillon, P. Poulin, W. Neri, A. G. Ewing and G. Safina, *Electrochimica Acta*, 2016, **210**, 622-629 [610.1016/j.electacta.2016.1005.1124](https://doi.org/610.1016/j.electacta.2016.1005.1124).
25. E. C. Dankoski and R. M. Wightman, *Frontiers in integrative neuroscience*, 2013, **7**, 44 <https://doi.org/10.3389/fnint.2013.00044>.
26. P. R. Patel, H. Zhang, M. T. Robbins, J. B. Nofar, S. P. Marshall, M. J. Kobylarek, T. D. Kozai, N. A. Kotov and C. A. Chestek, *Journal of neural engineering*, 2016, **13**, 066002 <https://doi.org/066010.061088/061741-062560/066013/066006/066002>.

- 1
2
3 27. H. N. Schwerdt, M. J. Kim, S. Amemori, D. Homma, T. Yoshida, H. Shimazu, H.
4 Yerramreddy, E. Karasan, R. Langer and A. M. Graybiel, *Lab on a Chip*, 2017, **17**, 1104-
5 1115 DOI: 1110.1039/C1106LC01398H
6
7 28. H. N. Schwerdt, M. Kim, E. Karasan, S. Amemori, D. Homma, H. Shimazu, T. Yoshida,
8 R. Langer, A. M. Graybiel and M. J. Cima, 2017.
9
10 29. D. Raju, A. Mendoza, P. Wonenberg, S. Mohanaraj, M. Sarbanes, C. Truong and A. G.
11 Zestos, *Analytical Methods*, 2019, **11**, 1620-1630 DOI: 1610.1039/C1628AY02737D.
12
13 30. I. M. Taylor, E. M. Robbins, K. A. Catt, P. A. Cody, C. L. Happe and X. T. Cui,
14 *Biosensors and Bioelectronics*, 2017, **89**, 400-410 doi: 410.1016/j.bios.2016.1005.1084.
15
16 31. R. F. Vreeland, C. W. Atcherley, W. S. Russell, J. Y. Xie, D. Lu, N. D. Laude, F. Porreca
17 and M. L. Heien, *Analytical chemistry*, 2015, **87**, 2600-2607 DOI: 2610.1021/ac502165f.
18
19 32. M. J. Peairs, A. E. Ross and B. J. Venton, *Analytical Methods*, 2011, **3**, 2379-2386 DOI:
20 2310.1039/C2371AY05348E.
21
22 33. L. Qi, E. Thomas, S. H. White, S. K. Smith, C. A. Lee, L. R. Wilson and L. A. Sombers,
23 *Analytical chemistry*, 2016, **88**, 8129-8136
24 <https://doi.org/8110.1021/acs.analchem.8126b01871>.
25
26 34. L. Zhou, H. Hou, H. Wei, L. Yao, L. Sun, P. Yu, B. Su and L. Mao, *Analytical chemistry*,
27 2019, **91**, 3645-3651 <https://doi.org/3610.1021/acs.analchem.3648b05658>.
28
29 35. J. G. Roberts and L. A. Sombers, *Analytical chemistry*, 2018, **90**, 490-504 DOI:
30 410.1021/acs.analchem.1027b04732
31
32
33 36. P. Puthongkham, C. Yang and B. J. Venton, *Electroanalysis*, 2018, **30**, 1073-1081
34 <https://doi.org/1010.1002/elan.201700667>.
35
36 37. A. G. Zestos, C. Yang, C. B. Jacobs, D. Hensley and B. J. Venton, *Analyst*, 2015, **140**,
37 7283-7292 DOI: 7210.1039/C7285AN01467K.
38
39 38. B. P. Jackson, S. M. Dietz and R. M. Wightman, *Analytical chemistry*, 1995, **67**, 1115-
40 1120 <https://doi.org/1110.1021/ac00102a00015>.
41
42 39. F.-M. Zhou, Y. Liang, R. Salas, L. Zhang, M. De Biasi and J. A. Dani, *Neuron*, 2005, **46**,
43 65-74 <https://doi.org/10.1016/j.neuron.2005.1002.1010>.
44
45 40. E. Castagnola, N. W. Vahidi, S. Nimbalkar, S. Rudraraju, M. Thielk, E. Zucchini, C. Cea,
46 S. Carli, T. Q. Gentner and D. Ricci, *MRS advances*, 2018, **3**, 1629 DOI:
47 1610.1557/adv.2018.1698.
48
49 41. N. W. Vahidi, S. Rudraraju, E. Castagnola, C. Cea, S. Nimbalkar, R. Hanna, R. Arvizu,
50 S. A. Dayeh, T. Q. Gentner and S. Kassegne, *Journal of Neural Engineering*, 2020, **17**
51 046005 <https://doi.org/046010.041088/041741-042552/ab046009b046005c>.
52
53 42. N. Goshi, E. Castagnola, M. Vomero, C. Gueli, C. Cea, E. Zucchini, D. Bjanec, E.
54 Maggolini, C. Moritz and S. Kassegne, *Journal of Micromechanics and*
55 *Microengineering*, 2018, **28**, 065009 <https://doi.org/065010.061088/061361-066439/aab065061>.
56
57 43. M. Vomero, E. Castagnola, F. Ciarpella, E. Maggolini, N. Goshi, E. Zucchini, S. Carli,
58 L. Fadiga, S. Kassegne and D. Ricci, *Scientific reports*, 2017, **7**, 1-14 doi:
59 10.1038/srep40332 (42017).
60
61 44. D. H. Kim, Y. Oh, H. Shin, C. Park, C. D. Blaha, K. E. Bennet, I. Y. Kim, K. H. Lee and
62 D. P. Jang, *Analytical Methods*, 2018, **10**, 2834-2843
63 <https://doi.org/2810.1039/C2838AY00352A>.

- 1
2
3 45. M. Vomero, P. Van Niekerk, V. Nguyen, N. Gong, M. Hirabayashi, A. Cinopri, K.
4 Logan, A. Moghadasi, P. Varma and S. Kassegne, *Journal of Micromechanics and*
5 *Microengineering*, 2016, **26**, 025018 [https://doi.org/025010.021088/020960-](https://doi.org/025010.021088/020960-021317/025026/025012/025018)
6 [021317/025026/025012/025018](https://doi.org/025010.021088/020960-021317/025026/025012/025018).
7
8 46. M. Hirabayashi, B. Mehta, N. W. Vahidi, A. Khosla and S. Kassegne, *Journal of*
9 *Micromechanics and Microengineering*, 2013, **23**, 115001
10 <https://doi.org/115010.111088/110960-111317/115023/115011/115001>.
11 47. M. K. Z. Pavel Takmakov, Richard B. Keithley, Elizabeth Bucher, Gregory S. McCarty,
12 and R. Mark Wightman, *Anal Chem.*, 2010, **82**, 9892-9900
13 <https://doi.org/9810.1021/ac102399n>.
14 48. A. C. Schmidt, X. Wang, Y. Zhu and L. A. Sombors, *ACS nano*, 2013, **7**, 7864-7873.
15 49. B. K. Swamy and B. J. Venton, *Analytical chemistry*, 2007, **79**, 744-750 DOI:
16 [710.1021/ac061820i](https://doi.org/10.1021/ac061820i).
17 50. S. K. Smith, S. P. Gosrani, C. A. Lee, G. S. McCarty and L. A. Sombors, *Analytical*
18 *chemistry*, 2018, **90**, 12994-12999
19 <https://doi.org/12910.11021/acs.analchem.12998b03694>.
20 51. D. C. Harris, *Quantitative chemical analysis*, Macmillan, 2010.
21 52. E. Castagnola, K. Woepfel, A. Golabchi, M. McGuier, N. Chodapaneedi, J. Metro, I. M.
22 Taylor and X. T. Cui, *Analyst*, 2020, **145**, 2612-2620.
23 53. E. Castagnola, E. M. Robbins, K. M. Woepfel, M. Mcguier, A. Golabchi, I. M. Taylor,
24 A. Michael and X. T. Cui, *Frontiers in Bioengineering and Biotechnology*, 2020, **8**, 1343.
25 54. A. Abdalla, A. West, Y. Jin, R. A. Saylor, B. Qiang, E. Peña, D. J. Linden, H. F. Nijhout,
26 M. C. Reed and J. Best, *Journal of neurochemistry*, 2020, **153**, 33-50.
27 55. A. J. G. I Mitch Taylor, SR Sesack, AC Michael, *Journal of neurochemistry*, 2012, **122**,
28 283-294.
29 56. K. M. N. I Mitch Taylor, Seth H Walters, Erika L Varner, Zhan Shu, Kathleen M
30 Bartlow, Andrea S Jaquins-Gerstl, Adrian C Michael, *Journal of neurochemistry*
31 2015, **133**, 522-531.
32 57. B. D. Bath, D. J. Michael, B. J. Trafton, J. D. Joseph, P. L. Runnels and R. M. Wightman,
33 *Analytical chemistry*, 2000, **72**, 5994-6002 <https://doi.org/5910.1021/ac000849y>.
34 58. B. J. Venton and R. M. Wightman, *Journal*, 2003, **75**, 414 A-421 A
35 <https://doi.org/410.1021/ac031421c>.
36 59. N. T. Rodeberg, J. A. Johnson, E. S. Bucher and R. M. Wightman, *ACS chemical*
37 *neuroscience*, 2016, **7**, 1508-1518 <https://doi.org/1510.1021/acschemneuro.1506b00142>.
38 60. B. J. Venton and Q. Cao, *Analyst*, 2020, **145**, 1158-1168
39 <https://doi.org/1110.1039/C1159AN01586H>.
40 61. M. R. Deakin, P. M. Kovach, K. Stutts and R. M. Wightman, *Analytical chemistry*, 1986,
41 **58**, 1474-1480.
42 62. B. J. Venton and Q. Cao, *Analyst*, 2020, **145**, 1158-1168.
43 63. M. R. Deakin, R. Wightman and C. Amatore, *Journal of electroanalytical chemistry and*
44 *interfacial electrochemistry*, 1986, **215**, 49-61.
45 64. M. Z. Wrona and G. Dryhurst, *Bioorganic Chemistry*, 1990, **18**, 291-317
46 [https://doi.org/210.1016/0045-2068\(1090\)90005-P](https://doi.org/210.1016/0045-2068(1090)90005-P).
47 65. A. N. Patel, P. R. Unwin and J. V. Macpherson, *Physical Chemistry Chemical Physics*,
48 2013, **15**, 18085-18092 DOI: 18010.11039/C18083CP53513D
49
50
51
52
53
54
55
56
57
58
59
60

- 1
2
3 66. N. Verbiese-Genard, J. Kauffmann, M. Hanocq and L. Molle, *Journal of*
4 *electroanalytical chemistry and interfacial electrochemistry*, 1984, **170**, 243-254
5 [https://doi.org/210.1016/0022-0728\(1084\)80047-80049](https://doi.org/210.1016/0022-0728(1084)80047-80049).
6
7 67. M. Z. Wrona and G. Dryhurst, *The Journal of Organic Chemistry*, 1987, **52**, 2817-2825
8 <https://doi.org/2810.1021/jo00389a00032>.
9
10 68. A. Mendoza, T. Asrat, F. Liu, P. Wonenberg and A. G. Zestos, *Sensors*, 2020, **20**, 1173
11 <https://doi.org/1110.3390/s20041173>.
12
13 69. R. D. Lama, K. Charlson, A. Anantharam and P. Hashemi, *Journal*, 2012, **84**,, 8096–
14 8101 <https://doi.org/8010.1021/ac301670h>.
15
16 70. A. G. Güell, K. E. Meadows, P. V. Dudin, N. Ebejer, J. C. Byers, J. V. Macpherson and
17 P. R. Unwin, *Faraday discussions*, 2014, **172**, 439-455
18 <https://doi.org/410.1039/C1034FD00054D>.
19
20 71. P. Hashemi, E. C. Dankoski, J. Petrovic, R. B. Keithley and R. Wightman, *Analytical*
21 *chemistry*, 2009, **81**, 9462-9471 <https://doi.org/9410.1021/ac9018846>.
22
23 72. C. Yang, E. Trikantopoulos, C. B. Jacobs and B. J. Venton, *Analytica chimica acta*,
24 2017, **965**, 1-8 doi: 10.1016/j.aca.2017.1001.1039.
25
26 73. C. J. Meunier, G. S. McCarty and L. A. Sombers, *Analytical chemistry*, 2019, **91**, 7319-
27 7327.
28
29 74. A. Hermans, R. B. Keithley, J. M. Kita, L. A. Sombers and R. M. Wightman, *Analytical*
30 *chemistry*, 2008, **80**, 4040-4048 <https://doi.org/4010.1021/ac800108j>.
31
32 75. M. L. Heien, P. E. Phillips, G. D. Stuber, A. T. Seipel and R. M. Wightman, *Analyst*,
33 2003, **128**, 1413-1419 <https://doi.org/1410.1039/B307024G>.
34
35 76. E. C. Dankoski and R. M. Wightman, *Frontiers in integrative neuroscience*, 2013, **7**, 44.
36
37 77. D. P. Jang, I. Kim, S.-Y. Chang, H.-K. Min, K. Arora, M. P. Marsh, S.-C. Hwang, C. J.
38 Kimble, K. E. Bennet and K. H. Lee, *Analyst*, 2012, **137**, 1428-1435 DOI:
39 1410.1039/C1422AN15912K.
40
41 78. J. A. Stamford, Z. L. Kruk and J. Millar, *Brain research*, 1990, **515**, 173-180.
42
43 79. G. G. Wildgoose, P. Abiman and R. G. Compton, *Journal of Materials Chemistry*, 2009,
44 **19**, 4875-4886.
45
46 80. K. Jurkiewicz, M. Pawlyta, D. Zygadło, D. Chrobak, S. Duber, R. Wrzalik, A. Ratuszna
47 and A. Burian, *Journal of materials science*, 2018, **53**, 3509-3523
48 <https://doi.org/3510.1007/s10853-10017-11753-10857>.
49
50 81. S. Sharma, C. S. Kumar, J. G. Korvink and C. Kübel, *Scientific reports*, 2018, **8**, 1-12
51 <https://doi.org/10.1038/s41598-41018-34644-41599>.
52
53 82. Z. Xu and C. Gao, *Materials Today*, 2015, **18**, 480-492.
54
55 83. G. Nava, J. Schwan, M. G. Boebinger, M. T. McDowell and L. Mangolini, *Nano letters*,
56 2019, **19**, 7236-7245 <https://doi.org/7210.1021/acs.nanolett.7239b02835>.
57
58 84. A. Woodard, K. Shojaei, G. Nava and L. Mangolini, *Plasma Chemistry and Plasma*
59 *Processing*, 2018, **38**, 683-694.
60
61 85. Y.-J. Lee, *Journal of nuclear materials*, 2004, **325**, 174-179
62 <https://doi.org/110.1016/j.jnucmat.2003.1012.1005>.
63
64 86. F. Tai, S.-C. Lee, J. Chen, C. Wei and S. Chang, *Journal of Raman Spectroscopy: An*
65 *International Journal for Original Work in all Aspects of Raman Spectroscopy, Including*
66 *Higher Order Processes, and also Brillouin and Rayleigh Scattering*, 2009, **40**, 1055-
67 1059.

- 1
2
3 87. A. C. Ferrari and J. Robertson, *Physical review B*, 2000, **61**, 14095
4 <https://doi.org/14010.11103/PhysRevB.14061.14095>.
5
6 88. S. F. TRAYNELIS, *pH and brain function*, 1998, 417.
7 89. H. W. Richter and W. H. Waddell, *Journal of the American Chemical Society*, 1983, **105**,
8 5434-5440.
9 90. S. Schindler and T. Bechtold, *Journal of Electroanalytical Chemistry*, 2019, **836**, 94-101
10 <https://doi.org/110.1016/j.jelechem.2019.1001.1069>.
11 91. M. K. Zachek, A. Hermans, R. M. Wightman and G. S. McCarty, *Journal of*
12 *Electroanalytical Chemistry*, 2008, **614**, 113-120
13 <https://doi.org/110.1016/j.jelechem.2007.1011.1007>.
14 92. C. Lentz, B. Samuel, H. Foley and M. Haque, *Journal of Nanomaterials*, 2011, **2011**.
15
16
17
18
19
20
21
22
23
24
25
26
27
28
29
30
31
32
33
34
35
36
37
38
39
40
41
42
43
44
45
46
47
48
49
50
51
52
53
54
55
56
57
58
59
60